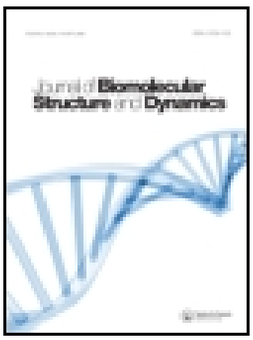

Taylor & Francis
Taylor & Francis Group

Journal of Biomolecular Structure and Dynamics

ISSN: 0739-1102 (Print) 1538-0254 (Online) Journal homepage: http://www.tandfonline.com/loi/tbsd20

Novel Coumarin Derivatives as Potent Acetylcholinesterase Inhibitors: Insight into Efficacy, Mode and Site of Inhibition

Prayasee Baruah, Grace Basumatary, Semen O. Yesylevskyy, Kripamoy Aguan, Ghanashyam Bez & Sivaprasad Mitra

To cite this article: Prayasee Baruah, Grace Basumatary, Semen O. Yesylevskyy, Kripamoy Aguan, Ghanashyam Bez & Sivaprasad Mitra (2018): Novel Coumarin Derivatives as Potent Acetylcholinesterase Inhibitors: Insight into Efficacy, Mode and Site of Inhibition, Journal of Biomolecular Structure and Dynamics, DOI: 10.1080/07391102.2018.1465853

To link to this article: https://doi.org/10.1080/07391102.2018.1465853

Accepted author version posted online: 17 Apr 2018.

Publisher: Taylor & Francis

Journal: *Journal of Biomolecular Structure and Dynamics*

DOI: http://doi.org/10.1080/07391102.2018.1465853

Novel Coumarin Derivatives as Potent Acetylcholinesterase Inhibitors: Insight into Efficacy, Mode and Site of Inhibition

Prayasee Baruah[1a], Grace Basumatary,[1a] Semen O. Yesylevskyy,[2] Kripamoy Aguan[1b], Ghanashyam Bez,[1a] and Sivaprasad Mitra[1a*]

[1]Centre for Advanced Studies in Chemistry and Department of Biotechnology & Bioinformatics, North-Eastern Hill University, Shillong – 793 022, India

[a]Centre for Advanced Studies in Chemistry; [b]Department of Biotechnology & Bioinformatics.

[2] Department of Physics of Biological Systems, Institute of Physics of the National Academy of Sciences of Ukraine, Prospect Nauky 46, 03028 Kyiv, Ukraine

*Author to whom all correspondence should be addressed. Phone: (91)-364-2722634. Fax: (91)-364-2550076. E-mail: smitra@nehu.ac.in, smitranehu@gmail.com.

Abstract: The inhibitory efficacy of two substituted coumarin derivatives on the activity of neurodegenerative enzyme acetylcholinesterase (AChE) was assessed in aqueous buffer as well as in the presence of human serum albumin (HSA) and compared against standard cholinergic AD drug, Donepezil (DON). The experimental data revealed the inhibition to be of non-competitive type with both the systems showing substantial inhibitory activity on AChE. In fact, one of the tested compounds Chromenyl Coumarate (CC) was found to be better inhibitor (IC_{50}= 48.49 ± 5.6 nM) than the reference drug DON (IC_{50} = 74.13 ± 8.3 nM), unequivocally amplifying its importance. The structure of the compound was found to play a vital role in the inhibitory efficiency, validating previous Structure Activity Relationship (SAR) reviews for coumarin. The mechanism of inhibition remained impervious when the experimental medium was switched from aqueous buffer to HSA, albeit noticeable change in the inhibition potency of the compound 3, 3'-Methylene-bis (4-hydroxy coumarin) (MHC) (38%) and CC (35%). Both the coumarin derivatives were observed to bind to the peripheral anionic site (PAS) of AChE and also found to displace the fluorescence marker thioflavinT (ThT) from AChE binding pocket. All experimental observations were seconded by molecular docking and MD simulation results. The inferences drawn in this study form a foundation for further investigation on these compounds; magnifying the probability of their usage as AD drugs and re-emphasizes the significance of drug delivery media while considering the inhibition potencies of targeted drugs.

Key-words: coumarin derivatives; AD drugs; acetylcholinesterase inhibition; human serum albumin; peripheral anionic site.

1. Introduction

Alzheimer's disease (AD), a chronic neurodegenerative disorder characterized by progressive cognitive and neuropsychiatric dysfunction, is the most prevalent form of dementia, accounting for roughly 60% of all types of dementia (Gard & Rusted, 2004; Kalaria et al., 2008). The alarmingly large number of populace impaired by the disease and its escalating growth rate have called for extensive research in discovering novel AD drugs with improved therapeutic effectiveness that could ameliorate and/or slowdown the progression of AD process (Ager et al., 2015; Wimo et al., 2017; Wimo, Jönsson, Bond, Prince, & Winblad, 2013). Several approaches have been undertaken to isolate/design novel drugs for the treatment of AD by exploring various AD-forming pathways. These include inhibition of both the AChE and Amyloid-beta (Aβ) pathways experimentally (Azam et al., 2017; Ferreira Neto et al., 2017; Gurung, Aguan, Mitra, & Bhattacharjee, 2016; Hojati, Ghahghaei, & Lagzian, 2017; Islam & Pillay, 2018) and also through pharmacophore screening (Iqbal, Anantha Krishnan, & Gunasekaran, 2017; Jafari et al., 2018; Malik, Choudhary, Srivastava, Mehta, & Sharma, 2017; Patel et al., 2017).

Acetylcholinesterase (AChE) is the enzyme involved in the termination of impulse transmission through rapid hydrolysis of the neurotransmitter acetylcholine (ACh), a progressive decline of which plays a key role in the pathogenesis of AD (Craig, Hong, & McDonald, 2011; Francis, Palmer, Snape, & Wilcock, 1999; Peters et al., 2012). Several drugs used in the treatment of AD are based on the established cholinergic hypothesis (Colovic, Krstic, Lazarevic-Pasti, Bondzic, & Vasic, 2013; McGleenon, Dynan, & Passmore, 1999), where the objective is to increase the concentration of ACh in the synaptic cleft by the inhibition of cholinesterase (ChE) activity. AChE inhibitors (AChEIs) impede the breakdown of the cholinesterase enzyme, augmenting the synaptic accessibility of ACh in the brain and subsequently boosting cholinergic

neurotransmission in forebrain regions that results in compensating the loss of functioning of brain cells. Owing to this, AChE inhibition has been documented as a critical treatment route of AD (Birks, 2006; McGleenon et al., 1999; Zemek et al., 2014).

AChEIs belong to myriad classes of structural and functional groups of compounds. However, numerous side effects of the available AD drugs have spurred the designing of novel AChEIs for pharmacological usage. The discovery of ensaculin (Hilgert, Nöldner, Chatterjee, & Klein, 1999; Hoerr & Noeldner, 2002), which is a coumarin derivative with piperazine ring having the ability to slow down the progression of AD led to the exploration of the efficacy of varied natural and synthetic coumarin derivatives as AChEIs. Coumarins are naturally occurring organic compounds which exhibit a variety of physiological and clinical applications with diverse effects, out of which AChE inhibition is one of the well-reported events (Jain & Joshi, 2012).

The crucial structural features of AChE consist of a catalytic active site (CAS) and a peripheral active site (PAS) connected by a narrow, yet deep (20 Å) gorge (Martis et al., 2015). The location of the CAS is near the bottom of the gorge; whereas, the PAS is situated near the enzyme surface (Colletier et al., 2006). The knowledge of inhibitor binding site is of primary importance for AChE, since the binding to the PAS has also been implicated in playing a role to decrease the aggregating effects of the enzyme on the amyloid peptide (Alvarez et al., 1995). A range of AChEIs have been developed for AD which can bind to the CAS, the PAS, or both (Castro & Martinez, 2001; Chen et al., 2015; Gupta & Mohan, 2014).

Coumarins are known to bind with the Peripheral Anionic Site (PAS) of AChE (Fallarero et al., 2008); but, functionalization of the coumarin heterocycles and substitution of the coumarin template, particularly at positions 3 and 4 with amine functional moiety including benzylamino,

phenylpiperazine or aniline groups using appropriate spacer, renders it capable of greater interaction on AChE, increasing the potency of inhibition (Anand, Singh, & Singh, 2012; Shen et al., 2005). Further, recent studies have also revealed that a large number of coumarin derivatives with a longer lateral chain promotes a good interaction with peripheral active site of AChE and hence represents the best inhibitory activity (de Souza, Rennã, & Figueroa-Villar, 2016). Nevertheless, irrespective of their binding site (CAS or PAS) with AChE, coumarins have shown promising activity as AChEIs. Further, it has also been reported that 4-hydroxycoumarin derivatives containing an amine functional group on alkyl side chain, particularly a tertiary amino group, show promising AChEI activity (Razavi et al., 2013). The detection of crucial structural features within the coumarin template and comprehensive reviews on SAR have helped in designing as well as synthesizing new coumarin analogues with enhanced AChE inhibitory activity.

Ellman's method (Ellman, Courtney, Andres, & Featherstone, 1961) remains the most popular avenue to assess the potency of newly developed AChEIs, where the enzymatic hydrolysis is normally carried out in a buffer solution of pH 8.0. However, considering the complex nature of the body fluid, experiments in aqueous buffer solution is considered to be an extremely simplified and crude model that is incapable of correctly predicting the potency as well as efficacy of an inhibitor over the existing drugs. Therefore, *in-vitro* experiments in presence of human serum albumin (HSA), a highly soluble negatively charged protein occupying almost 60% in blood plasma (Lexa, Dolghih, & Jacobson, 2014; Zunszain, Ghuman, McDonagh, & Curry, 2008) is considered to be more relevant and realistic. HSA plays the role of a transport protein (Zergani et al., 2012) and further finds its use clinically as a drug delivery system owing to the prospect of improved targeting and reducing the side effects (Yang, Zhang, & Liang,

2014). In our previous work, we have already reported the effect of HSA on some of the well-known AD drugs (Islam, Gurung, Bhattacharjee, Aguan, & Mitra, 2016).

In the current work, the inhibitory effect of a new 4-hydroxycoumarin derivative (6-amino-5-(3-(4-hydroxy-2-oxo-2H-chrome-3-yl)-2-phenylpropyl)-1,3-dimethylpyrimidine-2,4(1H,3H)-dione) containing amine functional groups (Chromenyl Coumarate, CC) on AChE activity is evaluated. The result is compared with another coumarin compound: 3, 3'- Methylene-bis (4-hydroxy coumarin), MHC which is basically two hydroxyl coumarin skeletons linked by a methylene group. The structures of both these systems are shown in Scheme - I.

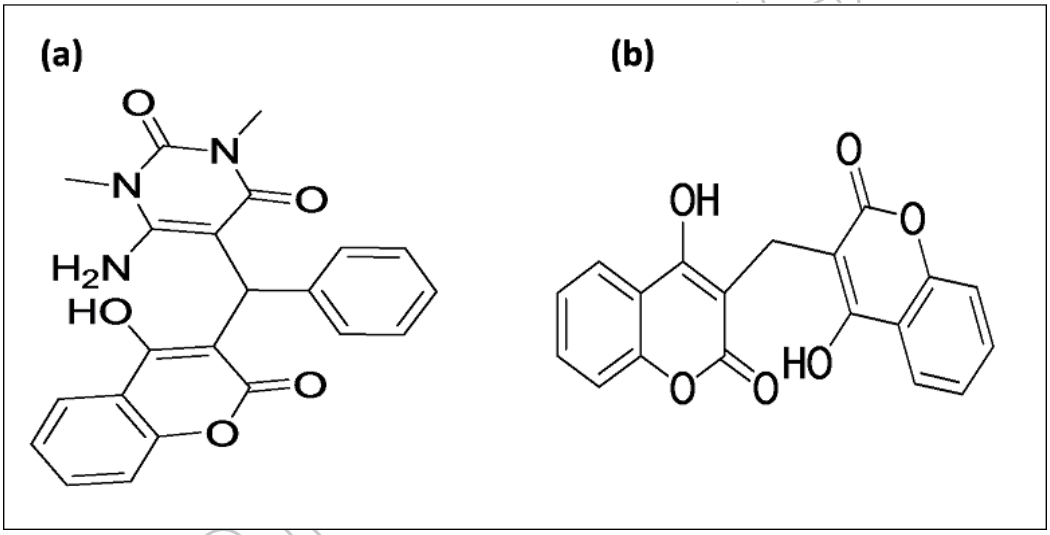

Scheme - I. The structures of the investigated systems: CC (a) and MHC (b)

The mechanism of binding as well as the efficacies of inhibition for both the coumarin derivatives have been evaluated against donepezil (DON), the most widely prescribed reversible AChE inhibitor, which has been found to be better tolerated amongst other known AChEIs with apparently less gastrointestinal side effects than rivastigmine or galanthamine (Tayeb, Yang, Price, & Tarazi, 2012). The results inferred are consequences of both enzyme kinetics as well as

fluorescence experiments. The mode of inhibition has been investigated from kinetic parameters in buffer solution and also in the presence of HSA under standard physiological condition. This study puts forward the possibility of these coumarin derivatives as potent new AChEIs taking into account of the substantial AChE inhibitory activities toward the treatment of AD through cholinergic pathway and also reinstates the modulations caused by the change in delivery media in determining their efficiency.

2. Experimental methods

2.1. Chemicals

Acetylcholinesterase (AChE) was purchased as type V-S, lyophilized powder from Electrophorus electricus (electric eel) with activity 1000 units/mg of protein, from Sigma Aldrich Chemical Company (cat. No. C2888). The reference inhibitor, Donepezil hydrochloride monohydrate (DON, purity 98% HPLC, cat no. D6821), the substrate acetylthiocholine iodide (purity 98% TLC powder or crystals cat no. A5751) and thioflavinT (ThT, cat. No. T3516) were also received from Sigma and used as received without any additional purification. Dithiobis (2-nitrobenzoic acid) (DTNB, the Ellman reagent) in the extra-pure form was procured from Sisco Research Laboratories (SRL), India (product no. 054817, 044883 and 1944142 respectively. Chromenyl Coumarate (CC) was synthesized following the protocol reported below; whereas, 3, 3' – Methylene-bis(4-hydroxy coumarin), MHC was obtained from Sigma Aldrich Chemical Company (cat. No.66762). Human Serum Albumin (HSA) was purchased as a fatty acid and globulin free, >99% (agarose gel electrophoresis) lyophilized powder (USB Corp. USA, cat. no. 10878 and was used as received. The gelatin used for preparing the AChE aliquots was received from Qualigens fine chemicals (a division of Glaxo Smithkline Pharmaceuticals Ltd., India). The analytical grade type II water used in carrying out the experiments (resistivity ~10 MΩ cm at

room temperature) was acquired from Elix 10 water purification system (Millipore India Pvt. Ltd.). Systronics μ-pH system 361 was used for checking the pH of the buffer solution.

2.2. Synthesis and characterization of CC

The compound CC was synthesized following the reported procedure (Bharti & Parvin, 2015) with slight modification. To an equimolar solution of 4-hydroxycoumarin (0.162 g, 1 mmol) and benzaldehyde (0.106 g, 1 mmol) in 1 mL ethanol, a solution of L-proline (0.023 g, 0.2 mmol) in water (0.2 mL) was added and stirred under reflux for 15 min. Then 6-amino-1,3-dimethyluracil (0.270 g, 1 mmol) was added to the reaction mixture and stirred for additional 5 h. The resulting mixture was cooled to room temperature, and the solid was filtered off and washed with water and ethanol to obtain the pure white solid product in 81% yield (0.328 g, 0.81 mmol). Melting point 215 °C; IR (KBr): 3434, 3245, 2955, 1666, 1617, 1569, 1542, 706 cm^{-1}; ^1H NMR (400 MHz, DMSO-d_6, δ ppm): 3.15 (s, 3H, -CH_3), 3.39 (s, 3H, -CH_3), 5.64 (s, 1H, -CH), 7.15-7.39 (m, 8H, ArH, -NH_2), 7.45 (d, *J*= 8 Hz, 1H, ArH), 7.66 (t, *J*= 8 Hz, 1H, ArH), 7.85 (d, J = 8 Hz, 1H, ArH), 14.0 (s, 1H, -OH); ^{13}C NMR (100 MHz, DMSO-d_6, δ ppm): 28.24, 30.58, 36.06, 74.91, 86.81, 104.65, 116.16, 116.95, 123.73, 124.33, 125.74, 126.38, 128.12, 132.44, 138.30, 150.07, 151.97, 155.17, 163.84, 164.10, 165.85. ESI-MS (*m*/*z*): 428 $[M+Na]^+$, 405 $[M]^+$. ^1H NMR, ^{13}C NMR and ESI-MZ spectra are represented in Fig. 1S – 3S in the supplementary section.

2.3. Measurement of AChE enzyme activity

Kinetic characterization of AChE was performed by following the method of Ellman et al. (1961) with slight modification in 0.1 M phosphate buffer of pH = 8.0at room temperature (298 K). The enzyme kinetics experiment in the absence and presence of HSA (concentration fixed at 250 μM) was carried out in synergy H1 hybrid meter plate reader instrument (BioTek) using 96

well plates. For both enzymatic and non-enzymatic studies, all the components of the reaction mixture were incubated for 5 min on ice cold water bath. The reaction was followed spectrophotometrically at 412 nm for 45 minutes inside the plate reader at the experimental temperature to follow the kinetics. The substrate concentration was varied from 50 μM to 2.0 mM in the experiments for measuring the kinetic parameters (Michaelis Menten constant, K_m and maximum hydrolysis rate, V_{max}) at two different inhibitor concentration. The effect of HSA on the IC_{50} values (concentration of the inhibitor at half maximal inhibition) of the inhibitor was checked by fixing the substrate concentration at the saturated condition of AChE catalysis reaction (~1.5 mM); while varying the inhibitor concentrations from very low till the saturation inhibition condition. The non-enzymatic hydrolysis reactions were performed by adding all the components except enzyme and were taken as corresponding blanks for the reaction. In both the non-enzymatic as well as enzymatic reactions, the concentration of DTNB was kept fixed at ~317 mM and the enzyme concentrations were ~0.079 units/ml in the enzymatic reactions. All the experimental results reported here are averaged for at least three independent sets.

2.4. Kinetic characterization for the enzyme catalysis and data analysis

The kinetic parameters were evaluated and data analysis was done using the Microcal Origin 2017 software. The non-enzymatic hydrolysis curve was subtracted off from the corresponding enzymatic hydrolysis curve and the initial linear portion of the progress curve considered for calculating the initial velocity of the reaction, V_0 by using Eq. (1).

$$\text{Initial rate, } V_0 \text{ (in moles per litre per second)} = \frac{\text{Slope}}{\epsilon \times l} \quad (1)$$

Where ε is the molar absorptivity of the yellow anion, (Pheifer & Briggs, 1995), l = 0.442 cm is the path length and the slope is in the units of absorbance per second. The enzyme kinetics was studied based on the kinetic scheme shown in Scheme - II.

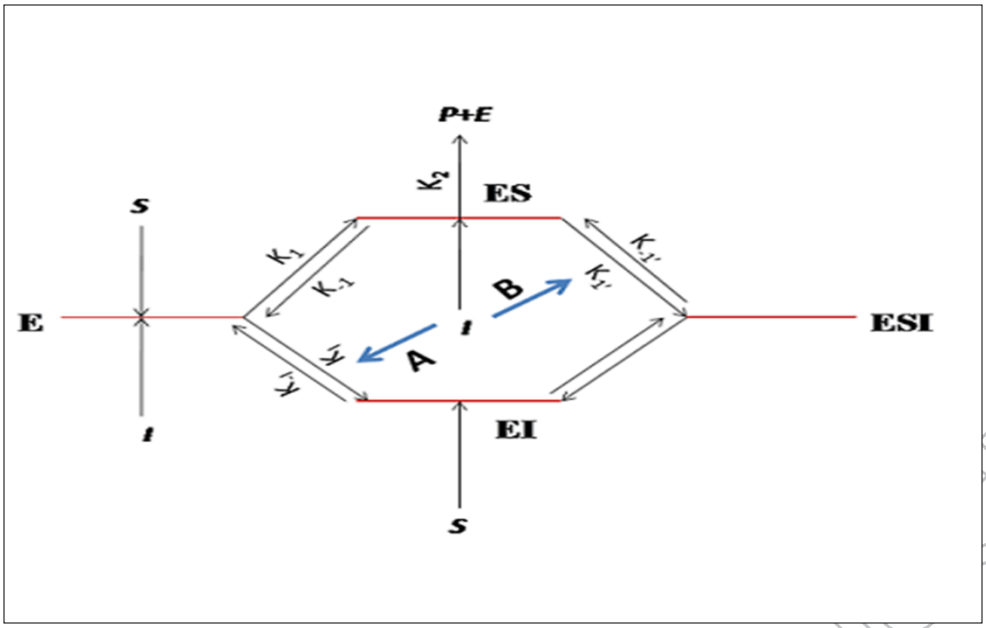

Scheme - II. The Michaelis-Menten scheme for enzyme catalysis and inhibition

Michaelis-Menten (MM) constant, K_m and maximum hydrolysis rate, V_{max} which are the standard measures for enzyme kinetics in biochemistry were obtained by non-linear regression analysis of the velocity (V_0) data against [S_0] with the relations corresponding to normal and inhibition cases given by Eq. 2a and 2b, respectively (Nelson & Cox, 2004).

$$V_0 = \frac{V_{max}[S_0]}{K_m + [S_0]} \qquad (2a)$$

$$V_0 = \frac{V_{max}'[S_0]}{K_m' + [S_0]} \qquad (2b)$$

Where the various terms are defined as follows:

$V_{max}' = \frac{V_{max}}{\alpha'}$, $K_m' = \frac{\alpha}{\alpha'} \times K_m$, or, $K_m' = \alpha \times K_m$ (for inhibition path A only);

$\alpha = 1 + \frac{[EI]}{[E]}$ and $\alpha' = 1 + \frac{[IES]}{[ES]}$ respectively (for both inhibition paths A and B)

The IC_{50} values of all the inhibitors both in absence and presence of HSA were calculated from the $K_{0.5}$ values by non-linear regression analysis using the modified Hill relation given in Eq. (3) (Copeland, 2005).

$$\frac{\Delta V}{\Delta V_{max}} = \frac{[I]^{n_H}}{K_{0.5}^{n_H} + [I]^{n_H}} \quad (3)$$

Where, ΔV represents the decrease in initial velocity in the presence of certain inhibitor concentration [I], and ΔV_{max} denotes the maximum decrease in initial velocity, $K_{0.5}$ is the concentration of the inhibitor that gives half-maximal initial velocity change and n_H is the Hill coefficient. The IC_{50} values were further verified by a non-linear regression of four parameter logistic plots (Volpe, Hamed, & Zhang, 2014) for individual drugs (not shown) and were found to be consistent with the values obtained from analysis of the modified Hill equation.

2.5. Fluorescence measurements

The medium used for the fluorescence measurements was 0.1 M phosphate buffer of pH 8.0. The solutions were prepared afresh and the spectroscopic measurements were performed after incubation of the solutions for sufficient time. Fluorescence spectral measurements were performed in Quanta Master (QM-40) steady state apparatus obtained from Photon Technology International (PTI) .The spectra were corrected for the instrument response function. Samples were excited at 412 nm for detecting the ThT fluorescence emission. The results were averaged from three separate experiments and analysed using Origin 2017 (Microcal Software, Inc., USA). Despite the compounds not having significant absorption at the excitation wavelength, the fluorescence spectra were corrected for any possible inner filter effect using the following equation (Islam, Sonu, Gashnga, Moyon, & Mitra, 2016):

$$F^{Corr}(\lambda_E, \lambda_F) = F_{Obs}(\lambda_E, \lambda_F) \times \frac{A(\lambda_E)}{A_{tot}(\lambda_E)} \quad (4)$$

Where A represents the absorbance of the free ThT, and A_{tot} is the total absorbance of the solution at the excitation wavelength (λ_E). After correction, the spectrum was considered to be the contribution from only ThT.

2.6. Molecular docking calculation

Molecular docking study was executed in two steps: the first step comprised of the protein and ligand molecules preparation which was followed by docking analysis. The 3D structures of the tested compounds were prepared using ChemDraw and optimized at the PM7 semi-empirical level of theory in Gaussian16 (Frisch et al. 2016) following the protocol described in the literature (Cazelli et al., 2017; Gonçalves et al., 2015). The 3D structures of AChE (PDB ID: 1C2O) and HSA (PDB ID: 1AO6) were retrieved from Protein Data Bank (www.rcsb.org). The protein preparation steps included the removal of all heteroatoms including ions and water molecules, addition of polar hydrogens and assignment of Kollmann charges using AutoDock tools-1.5.6 (ADT). The docking was executed using AutoDockVina (Trott & Olson, 2009) following the protocol of Lamarckian Genetic Algorithm (LGA) (Morris et al., 1998) for docking to protein targets. The detailed parameters for running the docking calculation are incorporated in the supplementary section.

Pymol was used for molecular visualization (Seeliger & De Groot, 2010). The conformational cluster analysis was done using maximum RMS tolerance of 2.00. Ten docking rounds were carried out for both the systems. The lowest energy conformer was chosen for modelling the docked images using Chimera (Pettersen et al, 2004) and Ligplot+ (Lakowski & Swindells, 2011) systems. The theoretically estimated inhibition constant (K_i) was calculated using Eq. 5; where, $\Delta G_{binding}$ (binding free energy) represents the sum of the inter- and

intramolecular enthalpies, R is the universal gas constant, and T denotes the temperature in Kelvin (Cazelli et al, 2017).

$$K_i = e^{\Delta G_{binding}/RT} \quad (5)$$

2.7. Molecular dynamics (MD) simulations

The best docking conformers of CC and MHC in complexes with AChE were used as input structures for MD simulations. Initial topologies of CC and MHC were generated by Acpype topology generator (da Silva & Vranken, 2012). The AMBER99 force field was used. The structures of both the ligands were optimized in Gaussian09 (Frisch et al, 2009) at the B3LYP/6-31G level of theory. The ESP partial charges were computed and added to initial topology. The charges of topologically equivalent atoms where averaged. All MD simulations were performed in Gromacs 5.1.2 package (Abraham et al, 2015). The protein-ligand complexes were solvated in truncated dodecahedron box containing ~13700 water molecules and 9 Na^+ ions, which balance the net negative charge of the protein. TIP3P water model was used. All simulations were performed in NPT conditions with the temperature 310 K and the pressure of 1 bar maintained by v-rescale thermostat and Berendsen barostat with isotropic pressure coupling respectively. The time step of 2 fs was used with all bonds converted to rigid constraints.

The following simulation protocol was used. On the first stage all heavy atoms of the protein and the ligands were restrained by harmonic restraints with the force constant of 1000 $kJ \cdot nm^{-2}$. The system was simulated for 2 ns to equilibrate water and ions. On the second stage only the atoms of protein backbone were restrained for 10 ns to equilibrate protein side chains and optimize position of the ligand accordingly. Finally, on the third stage free MD simulation without restraints was performed for 10 ns.

The stages 2 and 3 were used for analysis. The RMSDs of the ligands and protein heavy atoms and interaction energies between the ligands, protein and water were monitored. The energies were computed within the cutoff of 0.8 nm. Analysis of MD trajectories was performed with Pteros molecular modeling library (Yesylevskyy, 2012; Yesylevskyy, 2015).

3. Results and Discussion

3.1. Quantification of inhibitor potency in buffer medium

Both the investigated coumarin systems, viz. CC and MHC were found to exhibit inhibitory effect on the activity of free enzyme. An analysis of the kinetic parameters as well as the nature of Lineweaver-Burk (LB) plot point to the fact that the inhibition mechanism is analogous for all the tested systems. The inhibition, in all the three cases, is associated with the reduction of the V_{max} values while the magnitude of K_m remains unaltered; a condition characteristic of a non-competitive type of inhibition, which is known to be a special type of the mixed inhibition mechanism. In the non-competitive pathway, an inhibitor binds to the enzyme irrespective of whether the enzyme has bound to the substrate or not and hence involves both the inhibition pathways (marked A and B in Scheme - II), both of which are known to proceed simultaneously with comparable affinities. This process also renders identical values of α and α′. The MM as well as the LB plots is shown in Fig. 1 & Fig. 2, respectively.

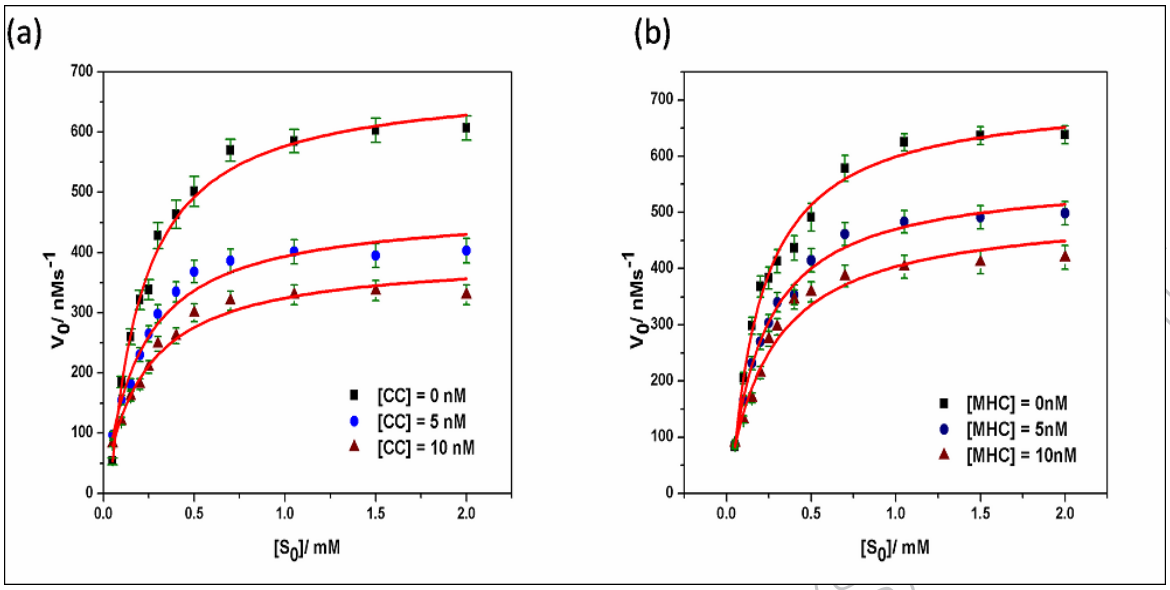

Fig. 1.Hydrolysis curve (scattered points) for AChE activity and its inhibition in presence of different concentrations of CC (a) and MHC (b) in phosphate buffer solution of pH = 8.0. The solid line represents non-linear regression of the experimental data points by Eq. (2). [AChE] = 0.079 u/ml.

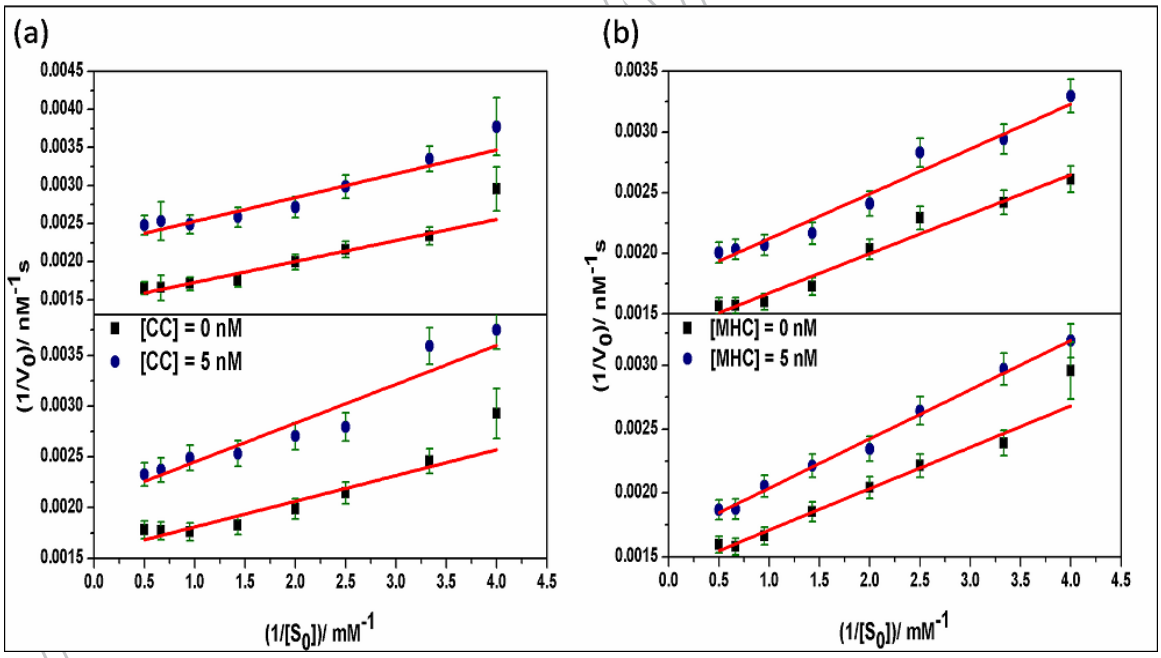

Fig 2. Lineweaver-Burk (LB) plot for the AChE hydrolysis data in aqueous buffer (a) and HSA medium (b) in absence and presence of CC and MHC.

DON was used as a reference compound and the results of kinetic analysis were found to be in good agreement with the previously published reports (Islam, et al., 2016; Mehta, Adem, & Sabbagh, 2012). The calculation of the IC_{50} values were done from the enzyme hydrolysis data (Fig. 3) using modified Hill relation given in Eq. 3. The kinetic results (Table 1) indicate that CC acts as the most potent AChE inhibitor with an IC_{50} value of 48.49±4.6 nM followed by MHC (80.16 ± 7.1 nM). All the compounds have been found to lower the AChE activity substantially with CC having an IC_{50} value even lower than DON (74.13 ± 8.3 nM), signifying its irrefutably strong potency towards AChE inhibition.

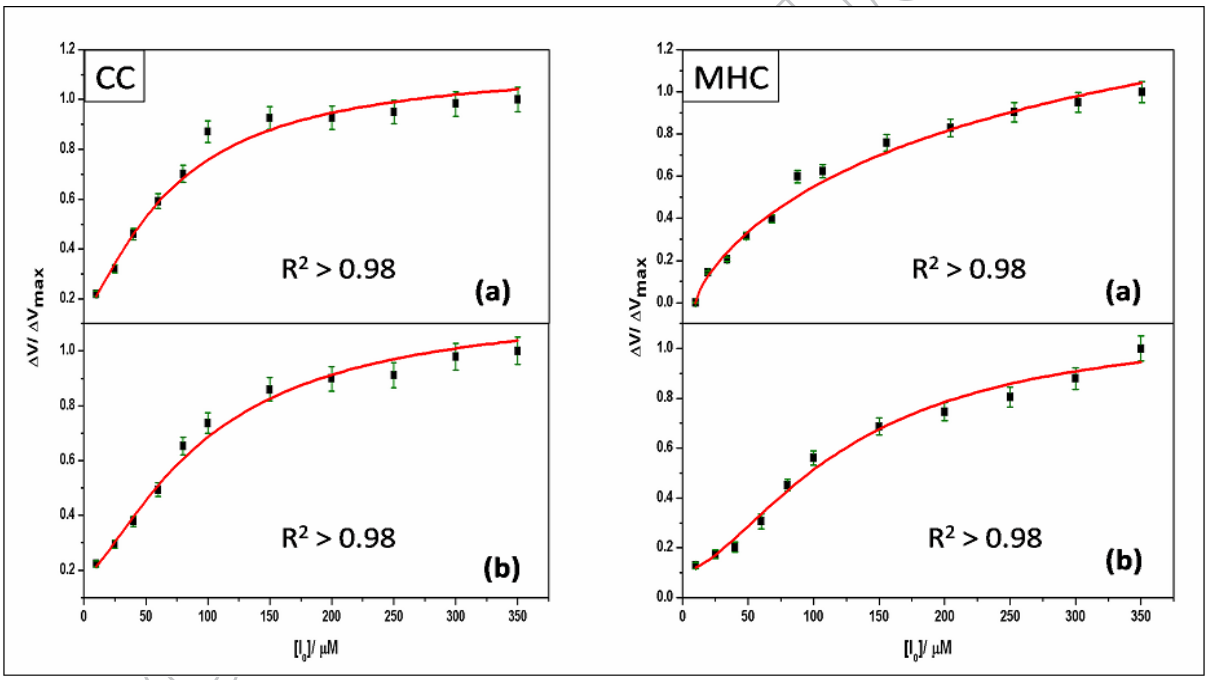

Fig. 3. Modified Hill analysis of AChE inhibition in aqueous buffer (a) and HSA medium (b) of CC and MHC.

The non-competitive mechanism is usually connected with binding at the PAS site of AChE, with Ethidium Bromide (EB) and Propidium Iodide (PI) being known examples in this category (Tong et al., 2013). Also in the present investigation, the molecular docking calculation for the action of the investigated coumarin derivatives on AChE confirms the binding site to be PAS (see molecular docking calculation results below). The PAS has been reported to be involved in substrate inhibition characteristics of AChE and binds ACh and other quaternary ligands, which act as uncompetitive inhibitors binding at a site separate from that occupied by the mono-quaternary competitive inhibitors (Colovic, et al., 2013). The presence of nitrogen containing moiety has been found to exhibit stronger interaction with AChE (Di Pietro et al., 2014; Pandolfi et al., 2017) and can explain the highest inhibitory potency of CC which is consistent with the experimental results reported here.

Table 1: Kinetic data of AChE hydrolysis and the effect of different concentration of inhibitors on various parameters in aqueous buffer medium.[a]

Systems	K_m/μM	V_{max}/nM s^{-1}	α	α'	IC_{50} (nM)	n_H
	From Michaelis Menten equation				From modified Hill equation	
AChE in presence of CC						
[CC] = 0 nM	141 ± 21	858 ± 42	1.0	1.0	48.49 ± 5.6	1.44 ± 0.1
[CC] = 5 nM	149 ± 27	498 ± 38	1.7	1.7		
[CC] = 10 nM	167 ± 30	401 ± 22	2.4	2.1		
AChE in presence of MHC						
[MHC] = 0 nM	170 ± 28	808 ± 26	1.0	1.0	80.16 ± 7.1	1.51 ± 0.1
[MHC] = 5 nM	174 ± 24	617 ± 24	1.3	1.3		
[MHC] =10 nM	166 ± 31	527 ± 37	1.5	1.5		

[a] [AChE] = 0.079 units/ ml

3.2. Quantification of inhibitor potency in presence of HSA

The modulation of drug efficiency in HSA, which is a highly versatile protein, is important in clinical diagnosis and is widely studied (Ariga, Naik, Nandibewoor, & Chimatadar, 2016; Jafari et al., 2018; Karthikeyan et al., 2017; Khan & Suresh Kumar, 2017; Wan et al., 2017) since serum albumin has been observed to bind compactly with drugs, even at very low concentration and it harbours multifunctional properties that are relevant to key pathologies underlying AD, including inhibition of the kinetics of Aβ fibrillation (Ezra, Rabinovich-Nikitin, Rabinovich-Toidman, & Solomon, 2015; Stanyon & Viles, 2012). It has been reported that low serum albumin level group of AD patients performed better in cognition level compared to higher serum level group (Llewellyn, Langa, Friedland, & Lang, 2010). To check the effect of HSA on AChE inhibition activity of the investigated compounds, the enzymatic reaction was monitored under the condition of fixed concentration of HSA (ca. 250 mM), which is close to the reported level of physiological abundance of serum albumins (Taverna, Marie, Mira, & Guidet, 2013). The control experiment was performed with free enzyme (without inhibitor) in presence of same concentration of the protein. In general, the inhibitory activity of both the compounds reduces significantly in presence of HSA with MHC being affected the most. However, LB analysis of the kinetic data indicates that the inhibition mechanism remains unaltered even in presence of HSA. The LB plots and the MM plots have been represented in Fig. 2 & Fig. 4, respectively whereas the corresponding kinetic parameters have been depicted in table 2.

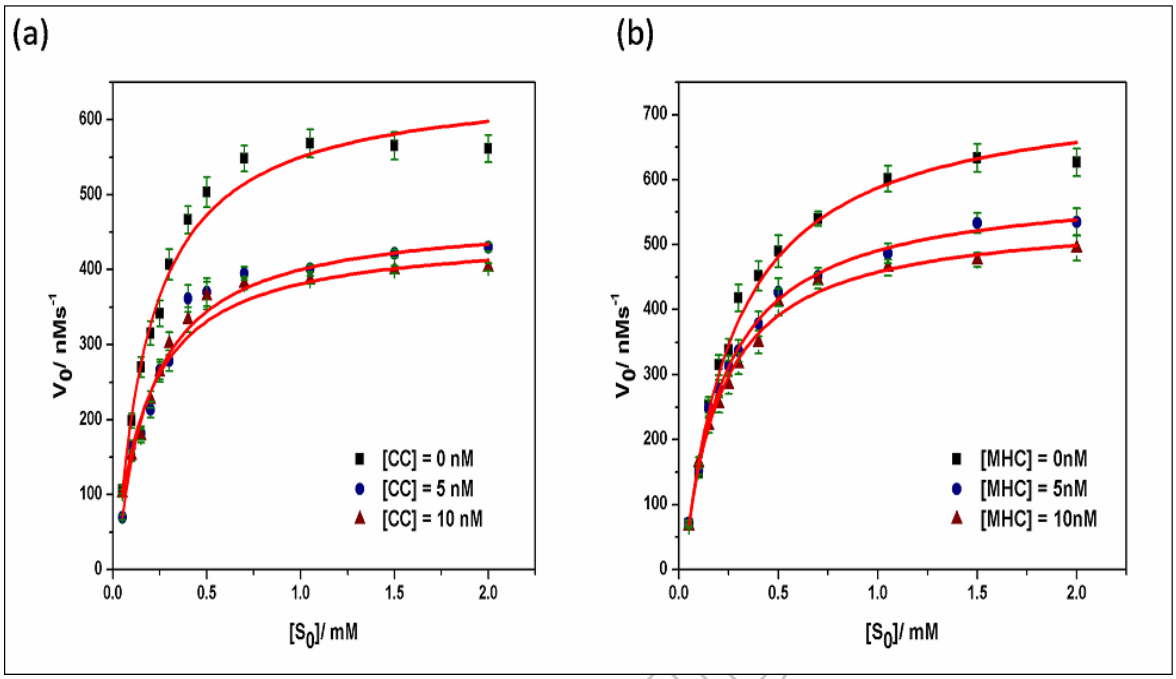

Fig. 4. Hydrolysis curve (scattered points) for AChE activity and its inhibition in presence of different concentrations of CC (a) and MHC (b) in HSA. The solid line represents non-linear regression of the experimental data points by Eq. (2). [AChE] = 0.079 u/ml.

Table 2: Kinetic data of AChE hydrolysis and the effect of different concentration of inhibitors on various parameters in HSA medium.[a]

Systems	K_m/μM	V_{max}/nM s^{-1}	α	α'	IC_{50} (nM)	n_H
	(From Michaelis Menten equation)				(From modified Hill equation)	
AChE in presence of CC						
[CC] = 0 nM	143 ± 17	784 ± 57	1.0	1.0	65.49 ± 8.0	1.40 ± 0.1
[CC] = 5 nM	158 ± 17	545 ± 30	1.5	1.5		
[CC] = 10 nM	156 ± 38	486 ± 38	1.7	1.6		
AChE in presence of MHC						
[MHC] = 0 nM	169 ± 23	825 ± 23	1.0	1.0	110.34 ± 11.6	1.51 ± 0.1
[MHC] = 5 nM	178 ± 17	667 ± 18	1.3	1.3		
[MHC] = 10 nM	174 ± 22	619 ± 22	1.4	1.4		

[a][AChE] = 0.079 units/ ml

The extent of reduction in the inhibition efficiency also varies significantly among different compounds. The comparative plot showing the Hill analysis of various inhibitors in presence of HSA is represented in Fig. 3. It is interesting to note that even in HSA medium, CC (IC_{50} = 65.49 ± 8.0 nM) shows greater capacity of inhibiting AChE activity than standard drug DON in aqueous medium (74.13 ± 8.32 nM). The kinetic parameters as well as the figures for analysis of inhibition potency of the reference compound (DON) have been given in the supplementary section (Table 1S & Figs. 4S – 6S, respectively).

The modulation of inhibition activity of the investigated coumarin systems in serum albumin matrix can be attributed to be due to the sequestration of the compounds by HSA and subsequent reduction in the availability of active fraction of the free inhibitor in solution (Islam, et al., 2016). The quantitative information on the binding affinities of the tested compounds can

be calculated by molecular docking studies, discussed later. Thus MHC, which binds with HSA more strongly, shows significant reduction of potency toward AChE inhibition in serum albumin, in comparison with its inhibition activity in aqueous buffer solution. The relative change in the IC_{50} values for all the compounds in HSA were calculated by using a protocol described earlier (Islam, et al., 2016) and were found to be 35% and 38% for CC and MHC respectively, which confirms the hypothesis proposed above.

3.3. Fluorescence spectral results

Thioflavin T is a well-known probe for monitoring AChE fluorescence. In one of our previous works, we have reported that the cholinergic drugs have a quenching effect on AChE bound ThT fluorescence (Islam & Mitra, 2016). In conformity with this observation, here too the two coumarin compounds exhibited quenching effect on ThT-AChE emission intensity. The extent of quenching was found to be more in case of CC (Fig. 7S) and consistent with the observations made from the kinetics experiments discussed in the previous section. The fluorescence excitation spectra of ThT-AChE binary system also remained unaltered with the addition of drug. The trends of the Stern-Volmer analysis using Eq. 5(a) are similar to those of the earlier reported cholinergic drugs and exhibit a downward curvature. The experimental data points did not show acceptable linear behaviour even when fitted with the modified Stern-Volmer equation (Eq. 5(b)).

$$\frac{F_0}{F} = 1 + K_{SV}[Q] \qquad 5\ (a)$$

$$\frac{F_0}{F_0 - F} = \frac{1}{f_a} + \frac{1}{f_a k_a [Q]} \qquad 5\ (b)$$

Hence, these synthesized coumarin compounds could be envisaged to follow a similar activity with those of standard AChEI drugs. The quenching of AChE bound ThT fluorescence in presence of these compounds can be cogitated to be the result of the partial replacement of ThT

from the AChE gorge to the aqueous buffer phase. From the kinetics experiment as well as molecular docking results to be discussed in the next section, CC and MHC have been found to have the tendency to bind at the peripheral anionic site (PAS) of the AChE binding region, thus hindering the approach of ACh enroute for its hydrolysis by the enzyme. Therefore, the coumarin compounds compete towards the AChE binding pocket and addition of these compounds in AChE – ThT system causes the substitution of a fraction of bound ThT from the AChE gorge. The compound CC, which possesses a greater affinity for AChE than ThT manages to displace ThT with ease, resulting in a sizeable decrease in fluorescence spectral intensity. On the other hand, MHC with a relatively lesser inhibitory effectiveness, reveals lesser degree of curvature (greater linearity) in the Stern-Volmer plots while evaluated against relatively strong inhibitor, CC. These results re-emphasize the validity of fluorimetric assay protocol for assessing the inhibition efficiency of the drugs. The results of the quenching experiments for the drugs with HSA are found to have good correlation with the kinetic results. For example, MHC shows a greater quenching efficiency than CC with representative K_{SV} (M^{-1}) values of $(5.9\pm0.21) \times 10^4$ and $(4.6\pm0.09) \times 10^4$ respectively, while considering the linear portion of the graph for individual systems. The emission spectra for the binding of MHC with ThT-AChE system and with HSA are given in Fig. 5; while the corresponding graphs for CC can be found in the supplementary section (Fig. 7S).

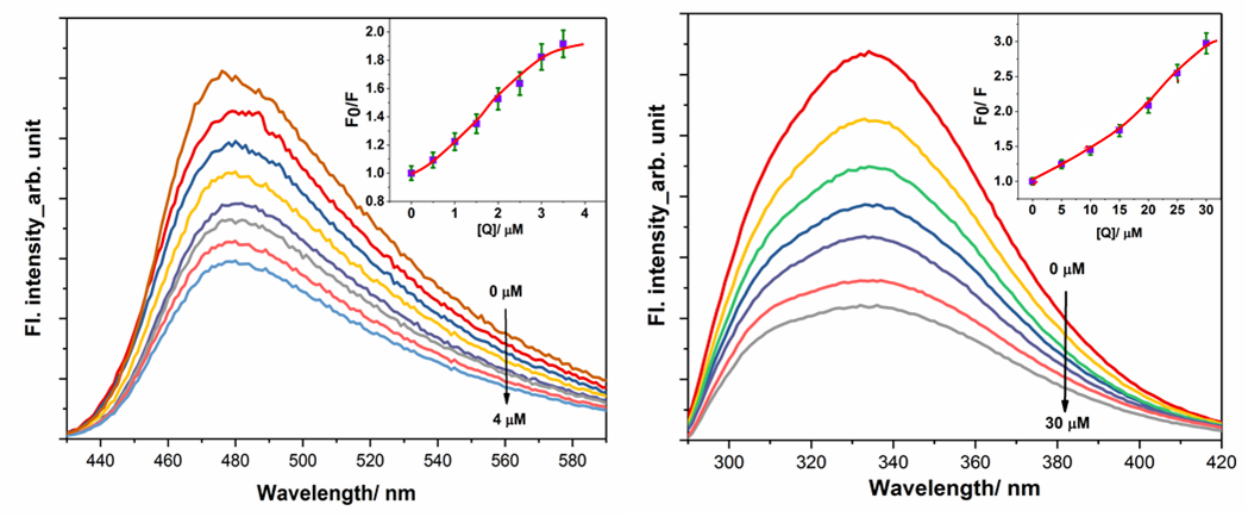

Fig 5. Quenching of emission intensity of ThT-AChE binary system (a) and HSA (b) in presence of increasing concentrations of MHC. Inset shows the Stern Volmer analysis.

3.4. Molecular Docking Results

3.4.1. Docking with AChE

The active site of AChE (catalytic site, CAS) consists of Ser 200, Glu 327 and His 440; whereas the peripheral anionic site (PAS) is characterized mainly by five amino acids—Tyr70, Asp72, Tyr121, Trp279 and Tyr334 (Bajda et al., 2013). The PAS is located at the entry to the active gorge and is responsible for extra activities, including the interaction with β-amyloid. Since the PAS is located on the enzyme surface, it directly occludes the active-site gorge. Thus, the binding of any ligand at this location would block the entry of substrates and the exit of products from the foot of the active site. This blockade can exhibit purposeful significance, as during ACh hydrolysis an incoming ACh molecule bound at PAS blocks the exit of produced choline molecule in active site, thus generating substrate inhibition (Dvir, Silman, Harel, Rosenberry & Sussman, 2010).

From the docking results, we have further validated our experimental findings as well as correlated the literature reports of general binding mode of coumarins with AChE. The docking images of both the compounds have been depicted in Fig 6.

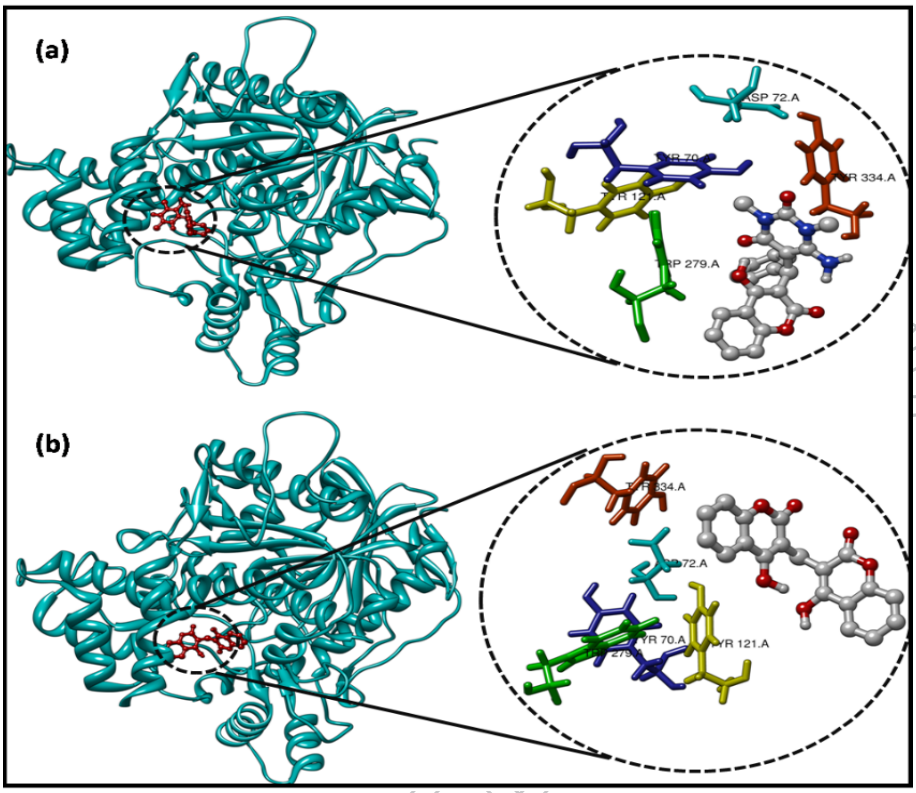

Fig 6. Lowest energy docked poses of CC (a) and MHC (b) with AChE. The binding site has been magnified for clarity.

From the docked pose, visual inspection conveys that neither of the ligands penetrates very deeply with the AChE gorge. Both the compounds have been found to bind at the periphery of the enzyme and in close contact with the residues characterizing the PAS (magnified in Fig 6), albeit in not the exact conformations. While considering a distance of 3.80 A, it was found that the ligands do not interact via hydrogen bonding or hydrophobic interactions with any residue of the active site gorge, despite being in close enough proximity to cause steric hindrance to the incoming substrate. The residues having closest contact are represented in table 3 and shown in

Fig. 8S. Atom O1 of CC is found to interact via H-bonding with His398 along with hydrophobic interactions whereas all interactions in case of MHC were found to be hydrophobic. CC is found to have the highest binding affinity with AChE (- 34.7 kJ/mol), followed by MHC (-33.0 kJ/mol) indicating CC to have a stronger binding with AChE. From docking, the binding energy of ThT was estimated to be 31.7 KJ/mol (Table 2S), which is very close to the binding affinities of CC and MHC. This provides the thermodynamic justification of the replacement of ThT in presence of inhibitors, as predicted by the fluorescence experimental results. The trend of inhibition constants remain the same from docking as obtained from experimental results.

3.4.2. Docking with HSA

The structure of HSA contains three homologous domains (named I, II, and III). Each domain contains two separate helical subdomains (named A and B), connected by random coil. The modular structural organization of HSA provides a variety of ligand binding site. Both CC and MHC have been found to bind at Domain I of HSA. While CC binds at domain IA, MHC has been found to bind at Domain IB of HSA with higher affinity. Table 3 and fig. 9S depict the residues in closest contact with the coumarins. The results indicate relatively stronger interaction of MHC with HSA (-38.51 kJ/mol) than CC (-37.52 kJ/mol). As in case of AChE, CC was found to form H-bonding with Leu115 and Arg117 through atoms O1 and O2 respectively in addition to hydrophobic interactions, whereas all interactions of MHC with its closest residues were hydrophobic in nature. The negative total free energy change observed for the interaction of all the tested compounds with AChE indicate a spontaneous binding and corroborate the experimentally observed inhibition behaviour of these inhibitors. Further, the binding affinity data given in Table 3 for the best pose structures of the inhibitors with AChE as well as with HSA, also predicts CC to be the most active AChE inhibitor, in conformity with the

experimental results discussed before. The corresponding parameters for some of the other poses are given in supplementary Table 3S.

Table 3. Binding affinities and other relevant parameters of the most stable docked pose of different inhibitors with HSA and AChE obtained from molecular docking calculation.

System	$\Delta G_{binding}$ (kJ/mol)	K_i (μM)	Binding Residues	
			H Bonding partners (distance, Å)	Hydrophobic
CC and AChE	-34.748	0.81	O1---His398 (3.17)	Trp524, Asn525, His406, Glu306, Pro232, Pro 403, Asn230
MHC and AChE	-33.069	1.59		His398, Trp524, Pro232, Pro403, Asn525, Asn230, His406,Glu306, Leu528, His362, Pro529, Leu532
CC and HSA	-37.255	0.29	O1---Leu115 (3.24) O2---Arg117 (3.27)	Tyr138, Met123, Leu182, Tyr161, Ile142, Gly189, Arg186, lys190, Arg145, Arg114
MHC and HSA	-38.512	0.17		Phe70, Ala26, Leu251, Leu66, Leu250,Leu22,Ala254, Pro152, Leu14, Arg10

3.5. Molecular Dynamics Simulations

Fig. 7(a) shows RMSD of the ligands and heavy atoms of AChE during MD simulations. It is clearly seen that during first 10 ns of simulation, when the protein backbone is restrained, the protein side chains evolve slightly from their positions in the crystal structure which results in RMSD of ~0.1 nm. The last 10 ns of simulation, which were performed without restraints, show increase of protein RMSD to ~0.2 nm. This value is very small for the protein of such significant size and indicates that the AChE structure is stable in water environment during MD simulations and remains close to its crystal structure.

Initial positions and conformations of the ligands obtained from docking evolve during the course of MD simulations. The CC ligand moves a bit away from its docking position and stabilizes at new conformation with average RMSD of ~0.8 nm from its initial structure. The behavior of MHC ligand is more complex. It shows several metastable states with different RMSD values but eventually also stabilize at conformation with RMSD of ~0.8 nm from its initial structure. Despite rather large deviations from initial docking conformations the final positions and orientations of the both ligands are remarkably stable.

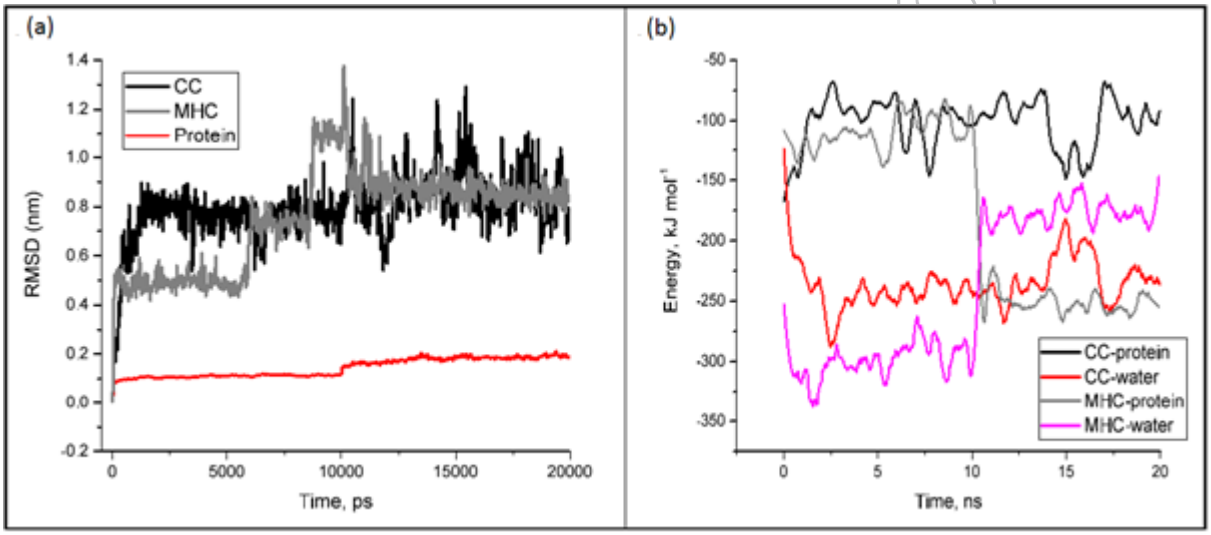

Fig 7: RMSD of ligands and heavy atoms of AChE (a) and evolution of interaction energy between ligands, AChE (protein) and water (b) during MD simulations. The curves on (b) are smoothed by running average method for clarity.

Fig. 7(b) shows evolution of interaction energy between the ligands, protein (AChE) and water during MD simulations. Both CC and MHC ligands initially have comparable interaction energy with protein, which is in agreement with their similar docking scores. The interaction of CC ligand with water becomes much stronger during the first 3 ns of simulation and then stabilizes at ca. -250 kJ/mol. In contrast, its interaction with AChE decreases from -150 kJ/mol to -100 kJ/mol. Several transient fluctuations are observed when the CC ligand binds stronger to

protein and lose contacts with water molecules. The MHC ligand behaves similar to CC during the first 10 ns of simulations when the protein backbone is restrained. After the release of this restraint, its interaction with protein increases dramatically and interaction with water decreases to the same extent. This means that the conformational mobility of the AChE backbone allows MHC to find more favorable binding position where it is better screened from water environment. However, no such behavior is observed for CC.

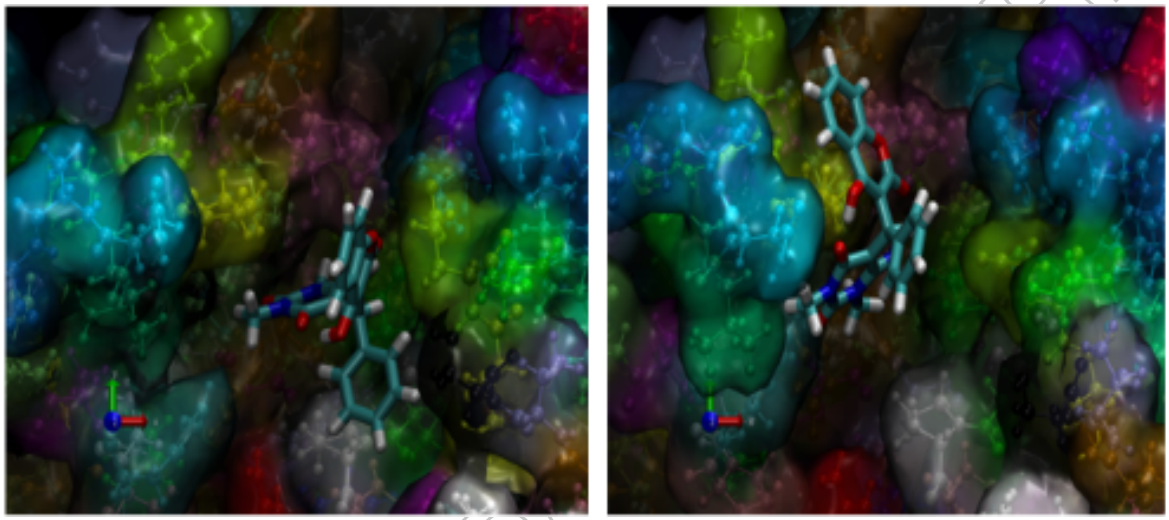

Fig 8. Initial position after docking (left) and equilibrated position after MD (right) for CC ligand. Each amino acid residue is shown in different color.

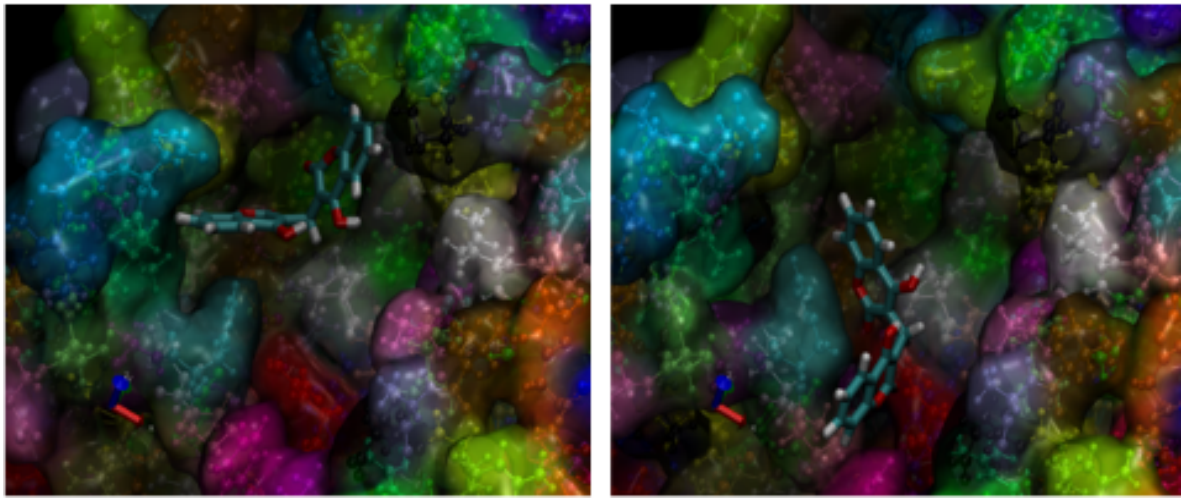

Fig 9. Initial position after docking (left) and equilibrated position after MD (right) for MHC ligand. Each amino acid residue is shown in different color.

Comparison of the best docking structures of the ligands and their final equilibrated conformations after MD simulations are shown in Figs 8 and 9. All-atom MD simulations in water environment confirm that both CC and MHC bind strongly to the binding site of AChE and remain stable there at the time scale of tens of nanoseconds. Equilibrated positions of both ligands in MD simulations are different from the lowest energy docking poses. The RMSDs between docking conformations and final MD structures are close to 0.8 nm for both ligands.

4. Conclusion

The inhibitory efficacies of two coumarin derivatives towards AChE were checked following Ellman's protocol and fluorescence measurements in conjunction with molecular docking as well as MD simulation results. Further, the modulatory effect of switching reaction medium from simple aqueous buffer to physiologically compatible serum matrix was also investigated. All the investigated systems were found to inhibit AChE in a non-competitive manner with CC showing the highest inhibition potency. Sequestration of the inhibitors by HSA rendered the reduction in AChE inhibition activity. Therefore, a potential AChEI is expected to have strong affinity to bind with AChE, but with lower tendency to be confiscated in HSA. Interestingly, one of the investigated systems (CC) showed greater inhibition potency even in presence HSA than standard cholinergic drug DON in free aqueous medium. Docking as well as MD result reveals that the binding of the coumarins with AChE to be strong and stable, which in turn could attribute towards their superior inhibitory potencies. The compounds were also found to displace ThT from AChE gorge, resulting in diminution of the emission intensity of ThT-AChE binary system and certifying the application of a fluorescence assay. These conjectures envisage the

potential application of these coumarin compounds with judicious synthetic fabrication as possible drug leads for the treatment of AD.

5. **Acknowledgements.** Financial support from Department of Biotechnology (BT/232/NE/TBP/2011) and Department of Science and Technology (SR/FST/CSI-194/2008), Govt. of India are gratefully acknowledged.

6. **Declaration of Interests.** The Authors declare that there are no competing interests associated with this manuscript.

References:

Abraham, M.J., et al. (2015) GROMACS: High performance molecular simulations through multi-level parallelism from laptops to supercomputers. *SoftwareX*, 1–2, 19-25. DOI: 10.1016/j.softx.2015.06.001

Ager, R. R., Davis, J. L., Agazaryan, A., Benavente, F., Poon, W. W., Laferla, F. M., & Blurton-Jones, M. (2015). Human neural stem cells improve cognition and promote synaptic growth in two complementary transgenic models of Alzheimer's disease and neuronal loss. *Hippocampus*, *25*, 813–826. DOI: 10.1002/hipo.22405

Alvarez, A., Bronfman, F., Pérez, C. A., Vicente, M., Garrido, J., & Inestrosa, N. C. (1995). Acetylcholinesterase, a senile plaque component, affects the fibrillogenesis of amyloid-β-peptides. *Neuroscience Letters*, *201*(1), 49–52. DOI: 10.1016/0304-3940(94)12127-C

Anand, P., Singh, B., & Singh, N. (2012). A review on coumarins as acetylcholinesterase inhibitors for Alzheimer's disease. *Bioorganic and Medicinal Chemistry*, *20*, 1175–1180. DOI: 10.1016/j.bmc.2011.12.042

Ariga, G. G., Naik, P. N., Nandibewoor, S. T., & Chimatadar, S. A. (2017). Quenching of fluorescence by meclizine, a probe study for structural and conformational changes in human serum albumin. *Journal of Biomolecular Structure and Dynamics*, *35*, 3161-3175. DOI: 10.1080/07391102.2016.1245159

Azam, F., Alabdullah, N. H., Ehmedat, H. M., Abulifa, A. R., Taban, I., & Upadhyayula, S. (2017). NSAIDs as potential treatment option for preventing amyloid β toxicity in Alzheimer's disease: an investigation by docking, molecular dynamics, and DFT studies. *Journal of Biomolecular Structure and Dynamics*. DOI: 10.1080/07391102.2017.1338164

Bajda, M., Więckowska, A., Hebda, M., Guzior, N., Sotriffer, C. A., & Malawska, B. (2013). Structure-based search for new inhibitors of cholinesterases. *International Journal of Molecular Sciences*, *14*, 5608–5632. DOI:10.3390/ijms14035608

Bharti, R. and Parvin, T. (2015) Molecular Diversity from the L-Proline catalyzed, Three-Component Reactions of 4-Hydroxycoumarin, Aldehyde, and 3- Aminopyrazole or 1,3-Dimethyl-6-Aminouracil. *Synthetic Communications, 45,* 1442–1450. DOI: 10.1080/00397911.2015.1023900

Birks, J. (2006). Cholinesterase inhibitors for Alzheimer's disease. *Cochrane Database of Systematic Reviews*, , Issue 1. Art. No.: CD005593. DOI: 10.1002/14651858.CD005593

Bourne, Y., Kolb, H. C., Radić, Z., Sharpless, K. B., Taylor, P., Marchot, P., Marchottll, P. (2017). Freeze-frame inhibitor captures acetyicholinesterase in a unique conformation, *Proc. Natl. Acad. Sci, 101*, 1449–1454. DOI: 10.1073/pnas.0308206100

Castro, A. & Martinez, A., (2001). Peripheral and dual binding site acetylcholinesterase inhibitors: implications in treatment of Alzheimer's disease. *Mini Reviews in Medicinal Chemistry*, *1*, 267–272. DOI : 10.2174/1389557013406864

Cazelli, D.S.P., Barroso, M.E.S., Pizi, R.B., Orlandi, M., De Souza, T.B., Carvalho, D.T., Goncalves A.S., Endringer, D.C. (2017) The relationship between the antimicrobial activity of eugenol and the LPETG peptide structure and associated analysis for docking purposes. *Chemical Papers*, *71*, 1877-1886. DOI: 10.1007/s11696-017-0181-0

Chen, Y., Liu, Z. L., Fu, T. M., Li, W., Xu, X. L., & Sun, H. P. (2015). Discovery of new acetylcholinesterase inhibitors with small core structures through shape-based virtual screening. *Bioorganic and Medicinal Chemistry Letters*, *25*, 3442–3446. DOI: 10.1016/j.bmcl.2015.07.026

Colletier, J.-P., Fournier, D., Greenblatt, H. M., Stojan, J., Sussman, J. L., Zaccai, G., Weik, M. (2006). Structural insights into substrate traffic and inhibition in acetylcholinesterase. *The EMBO Journal*, *25*, 2746–2756. DOI: 10.1038/sj.emboj.7601175

Colovic, M. B., Krstic, D. Z., Lazarevic-Pasti, T. D., Bondzic, A. M., & Vasic, V. M. (2013). Acetylcholinesterase Inhibitors: Pharmacology and Toxicology. *Current Neuropharmacology*, *11*, 315–335. DOI: 10.2174/1570159X11311030006

Copeland, R. A. (2013). Evaluation of Enzyme Inhibitors in Drug Discovery. A Guide for Medicinal Chemists and Pharmacologists. *Methods of Biochemical Analysis*. Vol. *46.* Wiley-Interscience, USA. ISBN 0-471-68696-4

Craig, L. A., Hong, N. S., & McDonald, R. J. (2011). Revisiting the cholinergic hypothesis in the development of Alzheimer's disease. *Neuroscience and Biobehavioral Reviews*, *35*, 1397–1409. DOI: 10.1016/j.neubiorev.2011.03.001

De Souza, L. G., Rennã, M. N., & Figueroa-Villar, J. D. (2016). Coumarins as cholinesterase inhibitors: A review. *Chemico-Biological Interactions*, *254*, 11–23. DOI: 10.1016/j.cbi.2016.05.001

Di Pietro, O., Viayna, E., Vicente-García, E., Bartolini, M., Ramón, R., Juárez-Jiménez, J., Muñoz-Torrero, D. (2014). 1,2,3,4-Tetrahydrobenzo[h][1,6]naphthyridines as a new family of potent peripheral-to-midgorge-site inhibitors of acetylcholinesterase: Synthesis, pharmacological evaluation and mechanistic studies. *European Journal of Medicinal Chemistry*, *73*, 141–152. DOI: 10.1016/j.ejmech.2013.12.008

Dvir, H., Silman, I., Harel, M., Rosenberry, T. L., & Sussman, J. L. (2010). Acetycholinesterase: From 3D Structure to Function. *Chemico-Biological Interactions*, *187*, 10–22. DOI: 10.1016/j.cbi.2010.01.042

Ellman, G. L., Courtney, K. D., Andres, V., & Featherstone, R. M. (1961). A new and rapid colorimetric determination of acetylcholinesterase activity. *Biochemical Pharmacology*, *7*, 88–95. DOI: 10.1016/0006-2952(61)90145-9

Ezra, A., Rabinovich-Nikitin, I., Rabinovich-Toidman, P., & Solomon, B. (2015). Multifunctional Effect of Human Serum Albumin Reduces Alzheimer's Disease Related Pathologies in the 3xTg Mouse Model. *Journal of Alzheimer's Disease*, *50*(1), 175–188. DOI: 10.3233/JAD-150694

Fallarero, A., Oinonen, P., Gupta, S., Blom, P., Galkin, A., Mohan, C. G., & Vuorela, P. M. (2008). Inhibition of acetylcholinesterase by coumarins: The case of coumarin 106.

Pharmacological Research, *58*, 215–221. DOI: 10.1016/j.phrs.2008.08.001

Ferreira Neto, D. C., Alencar Lima, J., Sobreiro Francisco Diz de Almeida, J., Costa França, T. C., Jorge do Nascimento, C., & Figueroa Villar, J. D. (2017). New semicarbazones as gorge-spanning ligands of acetylcholinesterase and potential new drugs against Alzheimer's disease: Synthesis, molecular modeling, NMR, and biological evaluation. *Journal of Biomolecular Structure and Dynamics*, DOI: 10.1080/07391102.2017.1407676

Francis, P. T., Palmer, A. M., Snape, M., & Wilcock, G. K. (1999). The cholinergic hypothesis of Alzheimer's disease : a review of progress. *J Neurol Neurosurg Psychiatry*, *66*, 137–147. PMID: 10071091

Frisch, M.J., et al., (2016) Gaussian 16. 2016, Gaussian, Inc.: Wallingford, CT, USA

Frisch, M.J., et al., (2009) Gaussian 09. 2009, Gaussian, Inc.: Wallingford, CT, USA

Gard, P. R., & Rusted, J. M. (2004). Angiotensin and Alzheimer's disease: Therapeutic prospects. *Expert Review of Neurotherapeutics*, *4*, 87–96. DOI: 10.1586/14737175.4.1.87

Gonçalves, A. S., França, T. C. C., de Oliveira, O. V. (2016). Computational studies of acetylcholinesterase complexed with fullerene derivatives: a new insight for Alzheimer disease treatment. *Journal of Biomolecular Structure and Dynamics*, *34*, 1307–1316. DOI: 10.1080/07391102.2015.1077345

Gupta, S., & Mohan, C. G. (2014). Dual Binding Site and Selective Acetylcholinesterase Inhibitors Derived from Integrated Pharmacophore Models and Sequential Virtual Screening, *BioMed Research International*, *2014,* 1-21. DOI: 10.1155/2014/291214

Gurung, A. B., Aguan, K., Mitra, S., & Bhattacharjee, A. (2017). Identification of molecular descriptors for design of novel Isoalloxazine derivatives as potential Acetylcholinesterase inhibitors against Alzheimer's disease. *Journal of Biomolecular Structure and Dynamics*, *35*, 1729-1742. DOI: 10.1080/07391102.2016.1192485

Halgren, T. A. (1996). Merck Molecular Force Field. *J. Comput. Chem.*, *17*(5–6), 490–519. DOI: 10.1002/(SICI)1096-987X(199604)17:5/6<490::AID-JCC1>3.0.CO;2-P

Hilgert, M., Nöldner, M., Chatterjee, S. S., & Klein, J. (1999). KA-672 inhibits rat brain acetylcholinesterase in vitro but not in vivo. *Neuroscience Letters*, *263*, 193–196. DOI: 10.1016/S0304-3940(99)00149-4

Hoerr, R., & Noeldner, M. (2002). Ensaculin (KA-672 HCl): a multitransmitter approach to dementia treatment. *CNS Drug Reviews*, *8*(2), 143–58. PMID: 12177685

Hojati, S., Ghahghaei, A., & Lagzian, M. (2017). The potential inhibitory effect of β-casein on the aggregation and deposition of Aβ $_{1-42}$ fibrils in Alzheimer's disease: insight from *in - vitro* and *in - silico* studies. *Journal of Biomolecular Structure and Dynamics*. DOI: 10.1080/07391102.2017.1345326

Iqbal, S., Anantha Krishnan, D., & Gunasekaran, K. (2017). Identification of potential PKC inhibitors through pharmacophore designing, 3D-QSAR and molecular dynamics simulations targeting Alzheimer's disease. *Journal of Biomolecular Structure and Dynamics*. DOI: 10.1080/07391102.2017.1406824

Islam, M. A., & Pillay, T. S. (2018). β-secretase inhibitors for Alzheimer's disease: identification using pharmacoinformatics. *Journal of Biomolecular Structure and Dynamics*. DOI: 10.1080/07391102.2018.1430619

Islam, M. M., Gurung, A. B., Bhattacharjee, A., Aguan, K., & Mitra, S. (2016). Human serum albumin reduces the potency of acetylcholinesterase inhibitor based drugs for Alzheimer's disease. *Chemico-Biological Interactions*, *249*, 1–9. DOI: 10.1016/j.cbi.2016.02.012

Islam, M. M., & Mitra, S. (2016). Cholinergic inhibitors replace thioflavin-T from acetylcholinesterase binding pocket: A potential fluorescence based molecular switch. *Chemical Physics Letters*, *664*, 63–69. DOI: 10.1016/j.cplett.2016.09.079

Islam, M. M., Sonu, V. K., Gashnga, P. M., Moyon, N. S., & Mitra, S. (2016). Caffeine and

sulfadiazine interact differently with human serum albumin: A combined fluorescence and molecular docking study. *Spectrochimica Acta - Part A: Molecular and Biomolecular Spectroscopy*, *152*, 23–33. DOI: 10.1016/j.saa.2015.07.051

Jafari, F., Samadi, S., Nowroozi, A., Sadrjavadi, K., Moradi, S., Ashrafi-Kooshk, M. R., & Shahlaei, M. (2018). Experimental and computational studies on the binding of diazinon to human serum albumin. *Journal of Biomolecular Structure and Dynamics*, *36*, 1490 - 1510. DOI: 10.1080/07391102.2017.1329096

Jain, P. K., & Joshi, H. (2012). Coumarin: Chemical and pharmacological profile. *Journal of Applied Pharmaceutical Science*, *2*(6), 236–240. DOI: 10.7324/JAPS.2012.2643

Kalaria, R. N., Maestre, G. E., Arizaga, R., Friedland, R. P., Galasko, D., Hall, K., Antuono, P. (2008). Alzheimer's disease and vascular dementia in developing countries: prevalence, management, and risk factors. *The Lancet Neurology*, *7*(9), 812–826. DOI: 10.1016/S1474-4422(08)70169-8

Karthikeyan, S., Bharanidharan, G., Mani, K. A., Srinivasan, N., Kesherwani, M., Velmurugan, D., Ganesan, S. (2017). Determination on the binding of thiadiazole derivative to human serum albumin: a spectroscopy and computational approach. *Journal of Biomolecular Structure and Dynamics*, *35*(4), 817–828. DOI: 10.1080/07391102.2016.1162751

Khan, A. Y., & Suresh Kumar, G. (2017). Exploring the binding interaction of potent anticancer drug topotecan with human serum albumin: spectroscopic, calorimetric and fibrillation study. *Journal of Biomolecular Structure and Dynamics*. DOI: 10.1080/07391102.2017.1359671

Laskowski, R.A., Swindells, M.B. (2011). LigPlot+: multiple ligand–protein interaction diagrams for drug discovery. *Journal of Chemical Informatics and Modelling* 51 (10) 2778–2786. DOI: 10.1021/ci200227u

Lexa, K. W., Dolghih, E., & Jacobson, M. P. (2014). A structure-based model for predicting serum albumin binding. *PLoS ONE*, *9*(4). DOI: 10.1371/journal.pone.0093323

Llewellyn, D. J., Langa, K. M., Friedland, R. P., & Lang, I. (2010). Serum albumin concentration and cognitive impairment. *Current Alzheimer Research*, *7*, 91–96. DOI : 10.2174/156720510790274392

Malik, R., Choudhary, B. S., Srivastava, S., Mehta, P., & Sharma, M. (2017). Identification of novel Acetylcholinesterase inhibitors through e-pharmacophore based virtual screening and molecular dynamics simulations. *Journal of Biomolecular Structure and Dynamics*, *35*, 3268–3284. DOI: 10.1080/07391102.2016.1253503

Martis, E. A. F., Chandarana, R. C., Shaikh, M. S., Ambre, P. K., Dsouza, J. S., Iyer, K. R., … Pissurlenkar, R. R. S. (2015). Quantifying ligand-receptor interactions for gorge-spanning acetylcholinesterase inhibitors for the treatment of Alzheimers disease. *Journal of Biomolecular Structure and Dynamics*, *33*(5), 1107–1125. DOI: 10.1080/07391102.2014.931824

McGleenon, B. M., Dynan, K. B. & Passmore. A. P. (1999). Acetylcholinesterase inhibitors in Alzheimer's disease. *British Journal of Clinical Pharmacology*, *48*, 471–480. DOI: 10.1046/j.1365-2125.1999.00026.x

Mehta, M., Adem, A., & Sabbagh, M. (2012). New acetylcholinesterase inhibitors for alzheimer's disease. *International Journal of Alzheimer's Disease*, *2012*. 1-8. DOI: 10.1155/2012/728983

Morris, G. M., Goodsell, D. S., Halliday, R. S., Huey, R., Hart, W. E., Belew, R. K., & Olson, A. J. (1998). Automated docking using a Lamarckian genetic algorithm and an empirical binding free energy function. *Journal of Computational Chemistry*, *19*, 1639–1662. DOI: 10.1002/(SICI)1096-987X(19981115)19:14<1639::AID-JCC10>3.0.CO;2-B

Nelson, D. L., & Cox, M. M. (2004). Lehninger Principles of Biochemistry, Fourth Edition. *W.H. Freeman*.

Pandolfi, F., De Vita, D., Bortolami, M., Coluccia, A., Di Santo, R., Costi, R., Scipione, L. (2017). New pyridine derivatives as inhibitors of acetylcholinesterase and amyloid aggregation. *European Journal of Medicinal Chemistry*, *141*, 197–210. DOI: 10.1016/j.ejmech.2017.09.022

Patel, C. N., Georrge, J. J., Modi, K. M., Narechania, M. B., Patel, D. P., Gonzalez, F. J., & Pandya, H. A. (2017). Pharmacophore-based virtual screening of catechol-o-methyltransferase (COMT) inhibitors to combat Alzheimer's disease. *Journal of Biomolecular Structure and Dynamics*. DOI: 10.1080/07391102.2017.1404931

Peters, J., Trovaslet, M., Trapp, M., Nachon, F., Hill, F., Royer, E., Tehei, M. (2012). Activity and molecular dynamics relationship within the family of human cholinesterases. *Physical Chemistry Chemical Physics*, *14*, 6764-6770. DOI: 10.1039/C2CP23817A

Pettersen, E.F., Goddard, T.D., Huang, C.C., Couch, G.S., Greenblatt, D.M., Meng, E.C., Ferrin, T.E. (2004) UCSF Chimera--a visualization system for exploratory research and analysis. *Journal of Computational Chemistry*, *25*, 1605-1612. DOI: 10.1002/jcc.20084

Pheifer, J.H. & Briggs, D.E. (1995). The estimation of thiols and disulphides in barley. *J. Inst. Brew. 101*, 5-10. DOI: 10.1002/j.2050-0416.1995.tb00843.x

Pissurlenkar, R. R. S. (2015). Quantifying ligand-receptor interactions for gorge-spanning acetylcholinesterase inhibitors for the treatment of Alzheimers disease. *Journal of Biomolecular Structure and Dynamics*, *33*, 1107–1125. DOI: 10.1080/07391102.2014.931824

Razavi, S. F., Khoobi, M., Nadri, H., Sakhteman, A., Moradi, A., Emami, S., Shafiee, A. (2013). Synthesis and evaluation of 4-substituted coumarins as novel acetylcholinesterase inhibitors. *European Journal of Medicinal Chemistry*, *64*, 252–259. DOI: 10.1016/j.ejmech.2013.03.021

Seeliger, D., & De Groot, B. L. (2010). Ligand docking and binding site analysis with PyMOL and Autodock/Vina. *Journal of Computer-Aided Molecular Design*, *24*(5), 417–422. DOI: 10.1007/s10822-010-9352-6

Shen, Q., Peng, Q., Shao, J., Liu, X., Huang, Z., Pu, X., Gu, L. (2005). Synthesis and biological evaluation of functionalized coumarins as acetylcholinesterase inhibitors. *European Journal of Medicinal Chemistry*, *40*, 1307–1315. DOI: 10.1016/j.ejmech.2005.07.014

Sousa da Silva, A.W., Vranken, W.F. (2012) ACPYPE - AnteChamber PYthon Parser interface. *BMC Research Notes*, 5, 367-374. DOI: 10.1186/1756-0500-5-367

Stanyon, H. F., & Viles, J. H. (2012). Human serum albumin can regulate amyloid-β peptide fiber growth in the brain interstitium: Implications for Alzheimer disease. *Journal of Biological Chemistry*, *287*(33), 28163–28168. DOI: 10.1074/jbc.C112.360800

Taverna, M., Marie, A.-L., Mira, J.-P., & Guidet, B. (2013). Specific antioxidant properties of human serum albumin. *Annals of Intensive Care*, *3*, 4. DOI: 10.1186/2110-5820-3-4

Tayeb, H. O., Yang, H. D., Price, B. H., & Tarazi, F. I. (2012). Pharmacotherapies for Alzheimer's disease: Beyond cholinesterase inhibitors. *Pharmacology and Therapeutics*, *134*, 8–25. DOI: 10.1016/j.pharmthera.2011.12.002

Tong, F., Islam, R. M., Carlier, P. R., Ma, M., Ekstrom, F., & Bloomquist, J. R. (2013). Effects of anticholinesterases on catalysis and induced conformational change of the peripheral anionic site of murine acetylcholinesterase. *Pesticide Biochemistry and Physiology*, *106*, 79–84. DOI: 10.1016/j.pestbp.2013.04.001

Trott, O., Olson, A.J. (2010) AutoDockVina: Improving the Speed and Accuracy of Docking with a New Scoring Function, Efficient Optimization, and Multithreading. *Journal of Computional Chemistry, 31*, 455-461. DOI: 10.1002/jcc.21334

Truhlar, D. G. (2009). Valence Bond Theory for Chemical Dynamics. *Journal of Computational Chemistry*, *28*, 73–86. DOI: 10.1002/jcc.20529

Volpe, D. A., Hamed, S. S., & Zhang, L. K. (2014). Use of Different Parameters and Equations for Calculation of IC50 Values in Efflux Assays: Potential Sources of Variability in IC50 Determination. *The AAPS Journal*, *16*, 172–180. DOI: DOI: 10.1208/s12248-013-9554-7

Wan, A., Miao, Y., Peng, L., Cai, Y., Chen, Y., He, Y., Li, H. (2017). Binding and biologic characterization of recombinant human serum albumin-eTGFBR2 fusion protein expressed in CHO cells. *Bioengineered*, *8*, 600–612. DOI: 10.1080/21655979.2017.1292186

Wimo, A., Guerchet, M., Ali, G. C., Wu, Y. T., Prina, A. M., Winblad, B., Prince, M. (2017). The worldwide costs of dementia 2015 and comparisons with 2010. *Alzheimer's and Dementia*, *13*, 1–7. DOI:10.1016/j.jalz.2016.07.150

Wimo, A., Jönsson, L., Bond, J., Prince, M., & Winblad, B. (2013). The worldwide economic impact of dementia 2010. *Alzheimer's and Dementia*, *9*, 1–11. DOI: 10.1016/j.jalz.2012.11.006

Yang, F., Zhang, Y., & Liang, H. (2014). Interactive association of drugs binding to human serum albumin. *International Journal of Molecular Sciences*, *15*, 3580–3595. DOI: 10.3390/ijms15033580

Yesylevskyy, S.O. (2012) Pteros: Fast and easy to use open-source C++ library for molecular analysis. *Journal of Computational Chemistry*, *33*, 1632-1636. DOI: 10.1002/jcc.22989

Yesylevskyy, S.O., (2015) Pteros 2.0: Evolution of the fast parallel molecular analysis library for C++ and python. *Journal of Computational Chemistry*, 36(19) 1480-1488. DOI: 10.1002/jcc.23943

Zemek, F., Drtinova, L., Nepovimova, E., Sepsova, V., Korabecny, J., Klimes, J., & Kuca, K. (2014). Outcomes of Alzheimer's disease therapy with acetylcholinesterase inhibitors and memantine. *Expert Opinion On Drug Safety*, *13*, 759–774. DOI: 10.1517/14740338.2014.914168

Zergani, F., Roohizadeh, R., Dayer, M.-R., Namdari, M., Farokhnia, A., Sobhany, Y., & Ghayour, O. (2012). In Silico Study of Global Structure of Human Serum Albumin. *International Journal of Green Nanotechnology*, *4*, 511–515. DOI: 10.1080/19430892.2012.739454

Zunszain, P. A., Ghuman, J., McDonagh, A. F., & Curry, S. (2008). Crystallographic Analysis of Human Serum Albumin Complexed with 4Z,15E-Bilirubin-IXα. *Journal of Molecular Biology*, *381*, 394–406. DOI: 10.1016/j.jmb.2008.06.016

SUPPLEMENTARY MATERIAL

associated with the manuscript

Novel Coumarin Derivatives as Potent Acetylcholinesterase Inhibitors: Insight into Efficacy, Mode and Site of Inhibition

Prayasee Baruah[1a], Grace Basumatary,[1a] Semen O. Yesylevskyy,[2] Kripamoy Aguan[1b], Ghanashyam Bez,[1a] and Sivaprasad Mitra[1a*]

[1]Centre for Advanced Studies in Chemistry and Department of Biotechnology & Bioinformatics, North-Eastern Hill University, Shillong – 793 022, India

[a]Centre for Advanced Studies in Chemistry; [b]Department of Biotechnology & Bioinformatics.

[2] Department of Physics of Biological Systems, Institute of Physics of the National Academy of Sciences of Ukraine, Prospect Nauky 46, 03028 Kyiv, Ukraine

Description of parameters used in molecular docking calculation

The following parameters were used for docking calculation: initial population size of 150, a maximum of 25,00,000 energy evaluations, mutation rate of 0.02 and a crossover rate of 0.8. The detection of ligand roots was done and the rotatable bonds were defined before docking. The grid size along the x-, y-, z-axes were set to 66 × 64 × 62 with a grid spacing of 1 Å, respectively. The grid box was centered at the coordinates x=5.059, y=65.057, z=56.351 for docking with AChE and 82×68×70 and x=25.304, y=9.525, z= 20.12for docking with HSA. For each ligand, number of docking run was set to 50.

Table 1S: Kinetic data of AChE hydrolysis and the effect of different concentration of Donepezil on various parameters in aqueous buffer media and HSA[a]

Systems	K_m/μM	V_{max}/nMs^{-1}	α	α'	IC_{50} (nM)	n_H
	From Michaelis Menten equation				From modified Hill equation	
Medium = aqueous buffer						
[DON] = 0 nM	146 ± 28	793 ± 47	1.0	1.0	74.13 ± 5.6	1.45 ± 0.1
[DON] = 5 nM	160 ± 36	550 ± 48	1.4	1.4		
[DON] =10 nM	138 ± 13	484 ± 15	1.5	1.6		
Medium = HSA						
[DON] = 0 nM	140 ± 32	794 ± 59	1.0	1.0	110.64 ± 12.1	1.51 ± 0.1
[DON] = 5 nM	163 ± 38	625 ± 42	1.4	1.4		
[DON] =10 nM	140 ± 26	571 ± 35	1.4	1.4		

[a] AchE = 0.079 units/ ml

Table 2S: Binding affinities of the docked poses of different inhibitors in decreasing stability.[a]

Mode	CC			MHC		
	Affinity ((kJ/ mol)	Distance from r.m.s.d lb	Distance from r.m.s.d ub	Affinity ((kJ/ mol)	Distance from r.m.s.d lb	Distance from r.m.s.d ub
Docked with AChE						
2	-36.82	0.80	6.91	-34.73	2.96	7.17
3	-35.98	1.42	3.16	-34.31	21.21	23.94
4	-35.14	1.70	7.32	-33.05	21.51	24.49
5	-35.14	19.1	21.09	-32.63	3.56	6.30
Docked with HSA						
2	-33.47	33.69	36.27	-35.14	0.71	2.08
3	-33.47	0.728	2.08	-34.73	0.81	2.09
4	-33.05	32.48	36.10	-33.89	3.62	5.43
5	-31.80	32.83	36.12	-33.89	3.81	8.04

[a] r.m.s.d is the root mean square deviation from lb (upper bound) and ub (upper bound)

Table 3S: Binding affinities of the docked poses of ThT with AChE in decreasing stability.[a]

Mode	ThT		
	Affinity ((kJ/mol)	Distance from r.m.s.d lb	Distance from r.m.s.d ub
1	-31.7	0.00	0.00
2	-30.5	2.28	3.03
3	-29.2	1.26	1.61
4	-28.8	2.22	8.13
5	-28.0	16.23	17.17

Supplementary figure captions:

Fig 1S: ^{1}H NMR spectra of Chromenyl Coumarate (CC).

Fig 2S: ^{13}C NMR spectra of Chromenyl Coumarate (CC).

Fig 3S: ES-MZ NMR spectra of Chromenyl Coumarate (CC).

Fig. 4S. Hydrolysis curve (scattered points) and Lineweaver-Burke (LB) plot for AChE activity and its inhibition in presence of different concentrations of DON in phosphate buffer solution of pH = 8.0. The solid line represents non-linear regression of the experimental data points by equation (2). [AChE] = 0.079 u/ml.

Fig. 5S. Hydrolysis curve (scattered points) and Lineweaver-Burke (LB) plot for AChE activity and its inhibition in presence of different concentrations of DON in HSA of pH = 8.0. The solid line represents non-linear regression of the experimental data points by equation (2). [AChE] = 0.079 u/ml.

Fig. 6S. Modified Hill analysis of AChE inhibition in aqueous buffer and HSA medium of DON.

Fig. 7S. Quenching of emission intensity of ThT-AChE binary system (a) and HSA (b) in presence of increasing concentrations of CC. Inset shows the Stern-Volmer analysis.

Fig. 8S. Pictorial diagr am representing the molecular interactions between CC and AChE. The dashed line indicates hydrogen bond whereas the arcs with radiating out spikes indicate hydrophobic interaction.

Fig 9S: Molecular interactions between CC and HSA. The dashed line indicates hydrogen bond whereas the arcs with radiating out spikes indicate hydrophobic interaction.

Fig. 1S

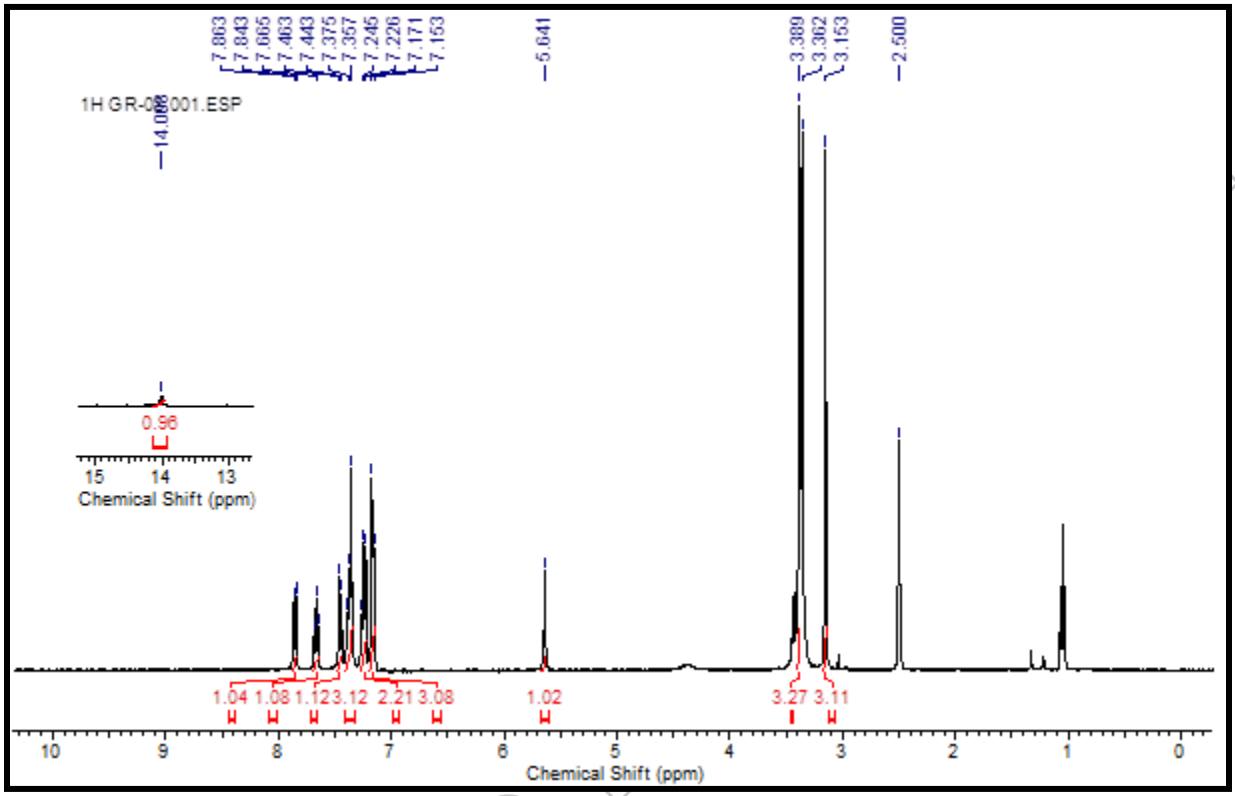

Fig. 2S

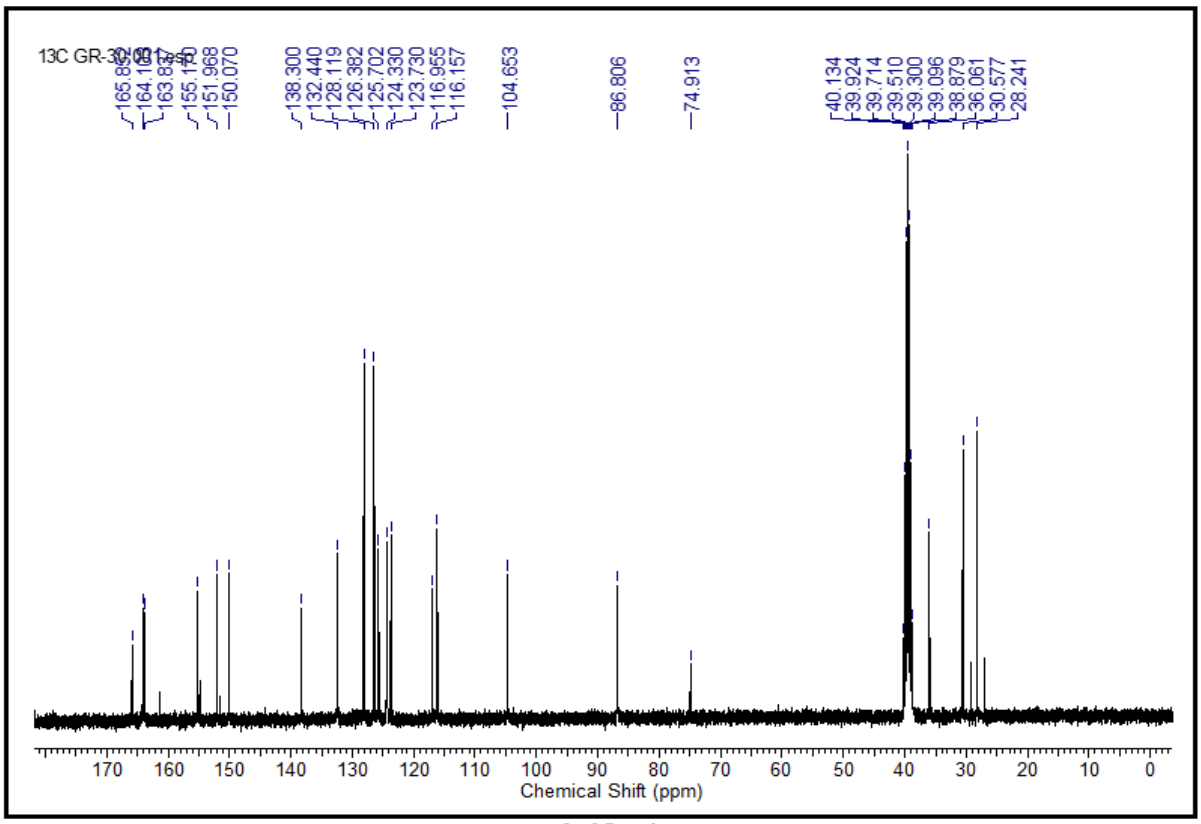

Fig. 3S

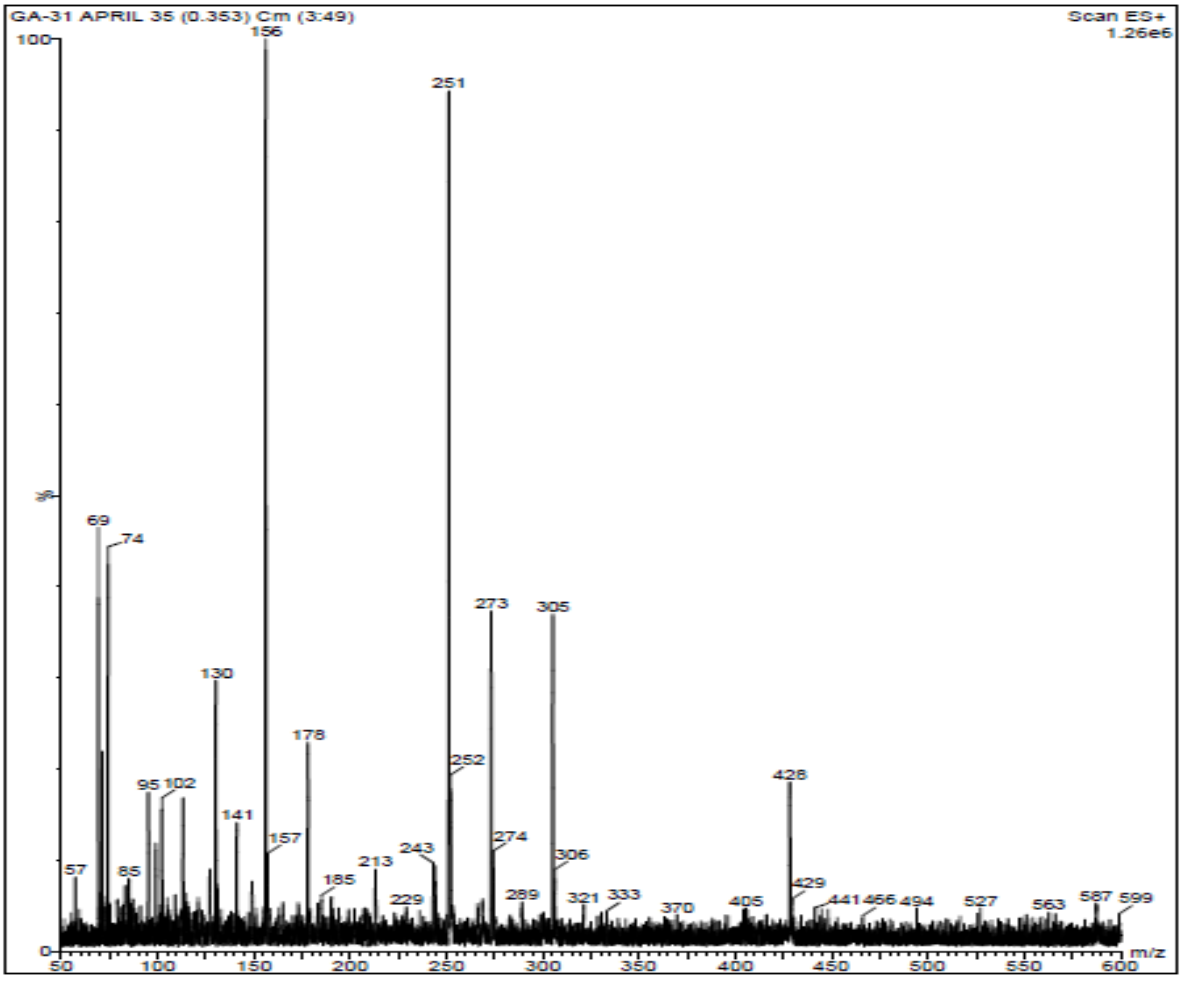

Fig. 4S

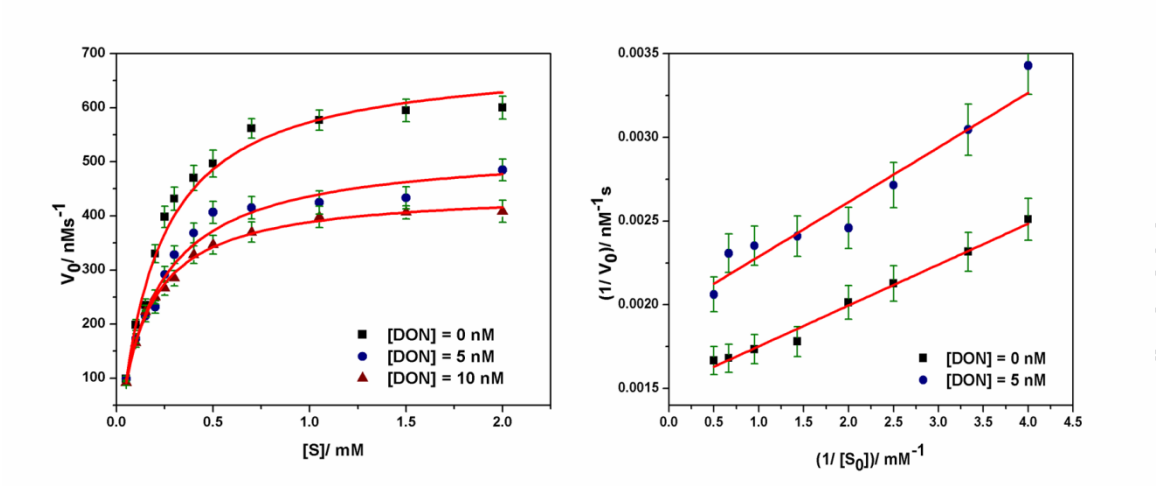

Fig. 5S

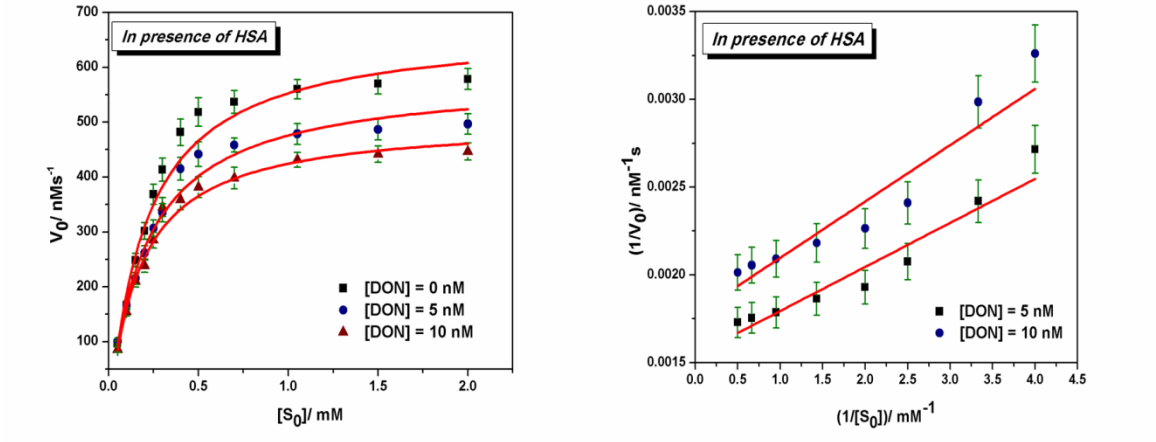

Fig. 6S

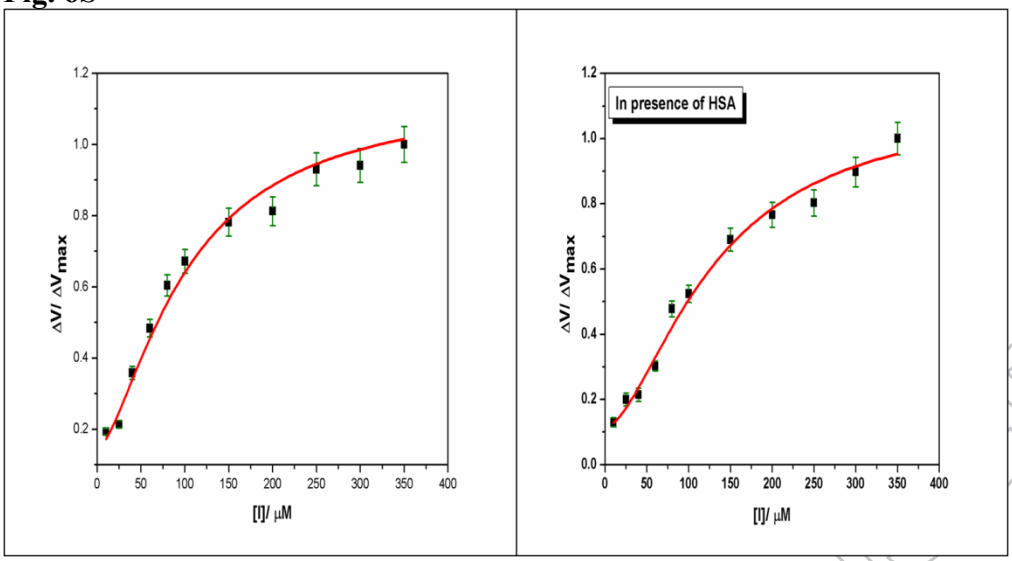

Fig. 7S

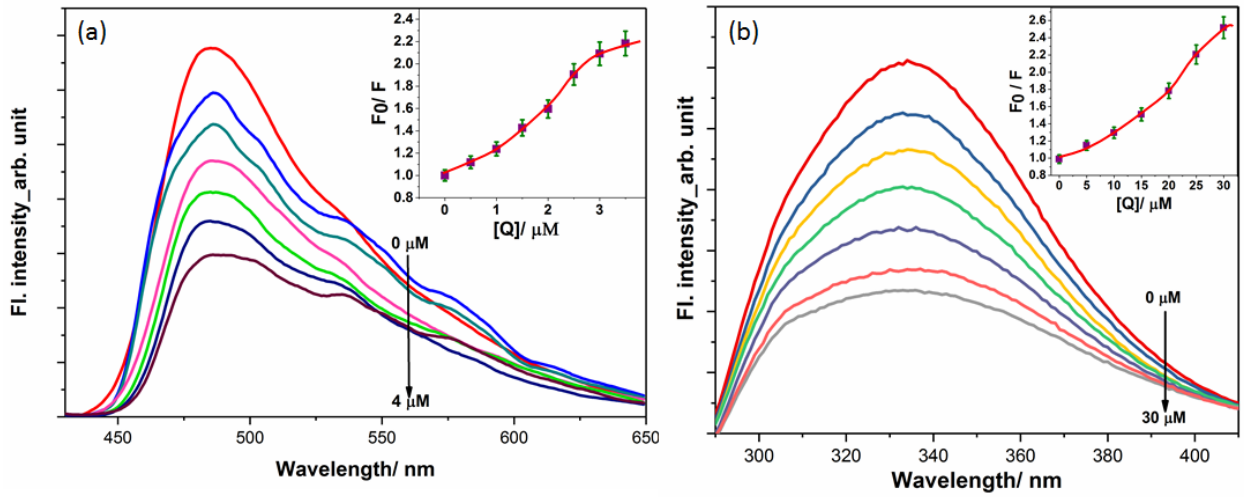

Fig. 8S

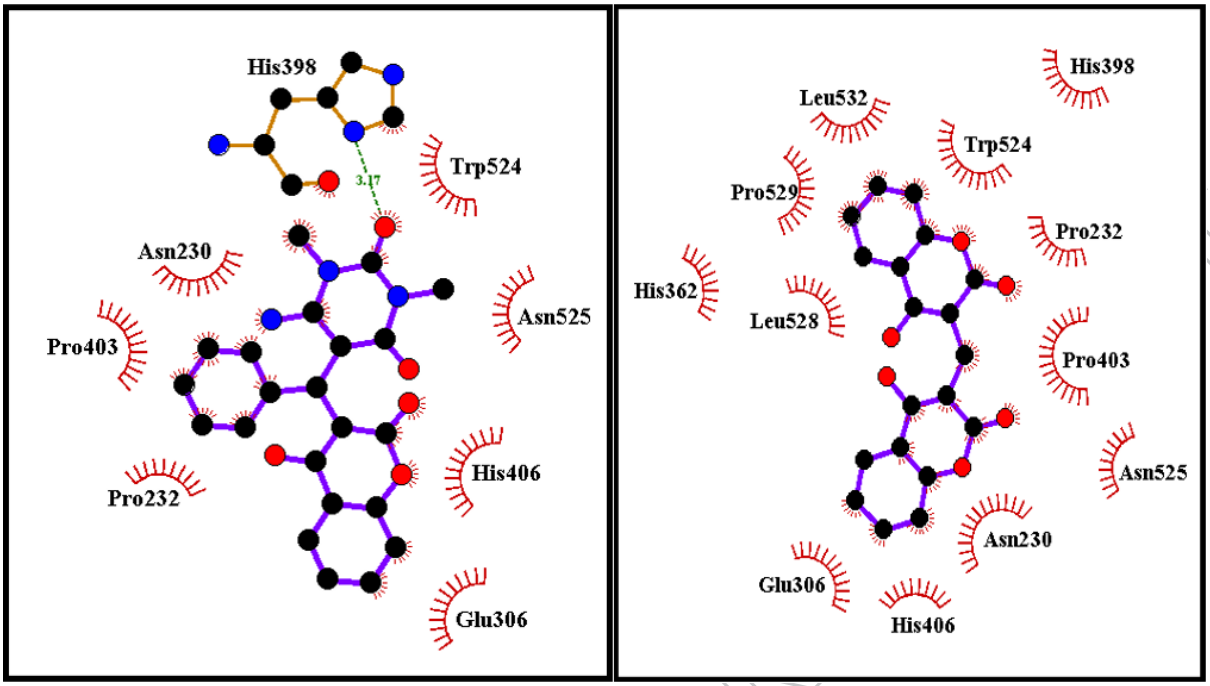
His398
Trp524
3.17
Asn230
Asn525
Pro403
His406
Pro232
Glu306
His398
Leu532
Trp524
Pro529
Pro232
His362
Leu528
Pro403
Asn525
Asn230
Glu306
His406

Fig. 9S

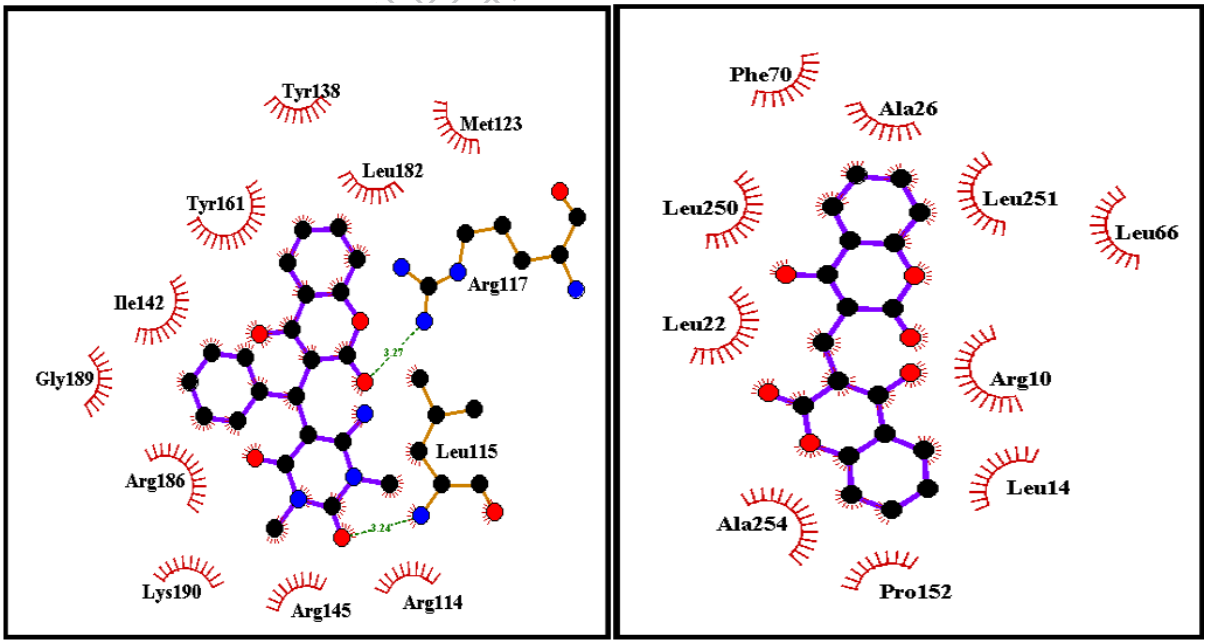
Tyr138
Met123
Leu182
Tyr161
Arg117
Ile142
3.27
Gly189
Leu115
Arg186
3.24
Lys190
Arg145
Arg114
Phe70
Ala26
Leu250
Leu251
Leu66
Leu22
Arg10
Leu14
Ala254
Pro152